NAVAL POSTGRADUATE SCHOOL
MONTEREY, CALIFORNIA

DTIC QUALITY INSPECTED

THESIS

INTEGRATED SYSTEM DAMPING AND
ISOLATION OF A THREE DIMENSIONAL
STRUCTURE

by

James A. Speer

March 1996

Thesis Advisor: Young S. Shin

19960806 011

REPORT DOCUMENTATION PAGE

Form Approved OMB No. 0704-0188

1. AGENCY USE ONLY *(Leave blank)*	2. REPORT DATE March 1996	3. REPORT TYPE AND DATES COVERED Master's Thesis

4. TITLE AND SUBTITLE INTEGATED SYSTEM DAMPING AND ISOLATION OF A THREE DIMENSIONAL STRUCTURE	5. FUNDING NUMBERS
6. AUTHOR(S): Speer,James,A.	
7. PERFORMING ORGANIZATION NAME(S) AND ADDRESS(ES) Naval Postgraduate School Monterey, CA 93943-5000	8. PERFORMING ORGANIZATION REPORT NUMBER
9. SPONSORING/MONITORING AGENCY NAME(S) AND ADDRESS(ES)	10. SPONSORING/MONITORING AGENCY REPORT NUMBER

11. SUPPLEMENTARY NOTES The views expressed in this thesis are those of the author and do not reflect the official policy or position of the Department of Defense or the U.S. Government.

12a. DISTRIBUTION/AVAILABILITY STATEMENT Approved for public release; distribution is unlimited.	12b. DISTRIBUTION CODE

13. ABSTRACT *(maximum 200 words)*

Controlling the vibratory response of a mechanical system is of key importance in most modern engineering designs. Constrained viscoelastic layered damping of vibrating elements is one method that can be used for vibration reduction. This thesis deals with an integrated system damping and excitation source isolation scheme of a three dimensional structure. Use of a validated finite element model of the system to predict system dynamic behavior proved to be an effective method in the design of the constrained viscoelastic layered damping treatment. Direct frequency response analysis was performed on the structure with the damping treatment applied and excitation source isolated. Experiments were also performed on the structure without the damping treatment tp provide reference data for comparison purposes.

14. SUBJECT TERMS Vibration, Vibration Damping, Viscoelastic Damping, Constrained Layered Damping, Vibration Isolation		15. NUMBER OF PAGES 86
		16. PRICE CODE

17. SECURITY CLASSIFICATION OF REPORT Unclassified	18. SECURITY CLASSIFICATION OF THIS PAGE Unclassified	19. SECURITY CLASSIFICATION OF ABSTRACT Unclassified	20. LIMITATION OF ABSTRACT UL

NSN 7540-01-280-5500

Standard Form 298 (Rev. 2-89)
Prescribed by ANSI Std. 239-18 298-102

INTEGRATED SYSTEM DAMPING AND ISOLATION OF A THREE DIMENSIONAL STRUCTURE

James A. Speer
Lieutenant Commander, United States Navy
B.S., Auburn University, 1983

Submitted in partial fulfillment
of the requirements for the degree of

## MASTER OF SCIENCE IN MECHANICAL ENGINEERING

from the

NAVAL POSTGRADUATE SCHOOL
March 1996
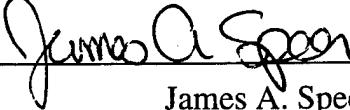
Author: _____
James A. Speer
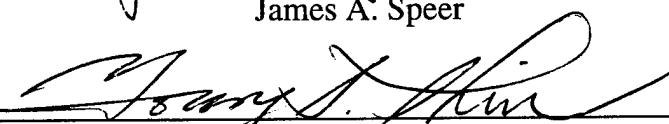
Approved by: _____
Young S. Shin, Thesis Advisor
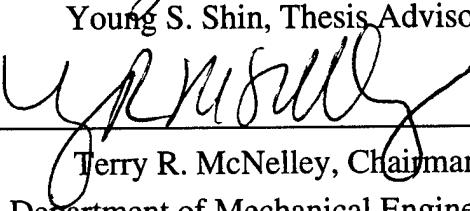
_____
Terry R. McNelley, Chairman
Department of Mechanical Engineering

ABSTRACT

Controlling the vibratory response of a mechanical system is of key importance in most modern engineering designs. Constrained viscoelastic layered damping of vibrating elements is one method that can be used for vibration reduction. This thesis deaks with an integrated system damping and excitation source isolation scheme for reducing the vibration signature of a three dimensional structure. Use of a validated finite element model of the system to predict system dynamic behavior proved to be an effective method in the design of the constrained viscoelastic layered damping treatment. Direct frequency response analysis was performed on the structure with the damping treatment applied and excitation source isolated. Experiments were also performed on the structure without the damping treatment to provide reference data for comparison purposes.

TABLE OF CONTENTS

ACKNOWLEDGMENTS

I would like to extend sincere thanks and gratitude to Professor Young S. Shin for his guidance and assistance in the performance of this research. I would also like to thank my wife, Rhonda, for her patience, support, and understanding.

x

I. INTRODUCTION

As the art of undersea warfare becomes more complex, the requirement for an increased acoustical advantage over the adversary becomes increasingly important. In order for a ship to remain acoustically quiet it must control its radiated noise signature. A major source of radiated noise onboard ships is the vibration of shipboard components.

In many practical situations, it is possible to reduce but not eliminate the dynamic forces that cause vibrations. Several methods can be used to control vibrations. A few of the more important ones are listed below [Ref. 1].

(1) Controlling the natural frequencies of the system and avoiding resonance under external excitation.

(2) Preventing excessive response of the system by introducing a damping or energy-dissipating mechanism.

(3) Reducing the transmission of the excitation forces from one part of the system to another by the use of vibration isolators.

(4) Reducing the response of the system by the addition of an auxiliary mass neutralizer or vibration absorber.

(5) Reducing the response of the system by the use of an active damping scheme.

Favorable vibration reductions have been achieved using various active damping strategies on flat panels and cantilever beams [Ref. 2, 3]. Passive damping has also proved to be an effective means of vibration reduction. Specifically, constrained viscoelastic layered damping shows much promise for vibration reduction over a broad frequency range. A study of the effects of various constrained viscoelastic layered damping treatments on flat plates is provided in references 4 and 5.

This thesis deals with the analysis and testing of an integrated constrained viscoelastic layered damping and source isolation scheme for a three dimensional system. The structure studied was a five sided aluminum box connected at the edges with weld

1

joints. Analysis and experimentation on the structure was limited to a frequency range of 0 to 100 hertz (Hz). For our system, this frequency range contained 20 vibration modes (6 rigid body and 14 elastic) which were the most pronounced in terms of dominating the system dynamic response. Utilization of a three dimensional structure provided the opportunity to conduct damping analysis/experiments on a system with complex mode shapes due to the simultaneous interaction of multiple sides.

II. THEORY

A. VISCOELASTIC MATERIAL

Viscoelastic damping capability is exhibited strongly in many polymeric and glassy materials [Ref. 6]. Polymeric materials are made up of long chains of carbon atoms which are joined strongly together. When these chains are linked to other similar chains a polymer network is developed. The damping action occurs during relaxation and recovery of the network after deformation has occurred.

An understanding of the variation of damping properties with the environment is essential for effective noise and vibration control treatments to be designed [Ref. 6]. Three factors which affect the properties of viscoelastic damping material are temperature, frequency, and cyclic strain amplitude. Of these three, temperature is considered to be the most significant. This temperature effect is illustrated in Figure 2.1. This figure highlights four distinct regions. In the glassy region, the storage modulus is at a maximum value while the loss factor is at a minimum. As temperature increases into the transition region, the storage modulus decreases while the loss factor increases to a peak value and starts to drop off. In the rubberlike region, the storage modulus and loss factor remain essentially constant at low values. As temperature increases into the flow region, storage modulus starts to decrease and the loss factor increases. It should be noted for most polymeric materials the flow region does not exist. Additionally, the width of the transition and rubberlike region can vary anywhere from 20 to 300 degrees C [Ref. 6].

Storage module E or loss factor η

E

η

Constant
Frequency

Glassy region | Transition region | Rubberlike region | Flow region
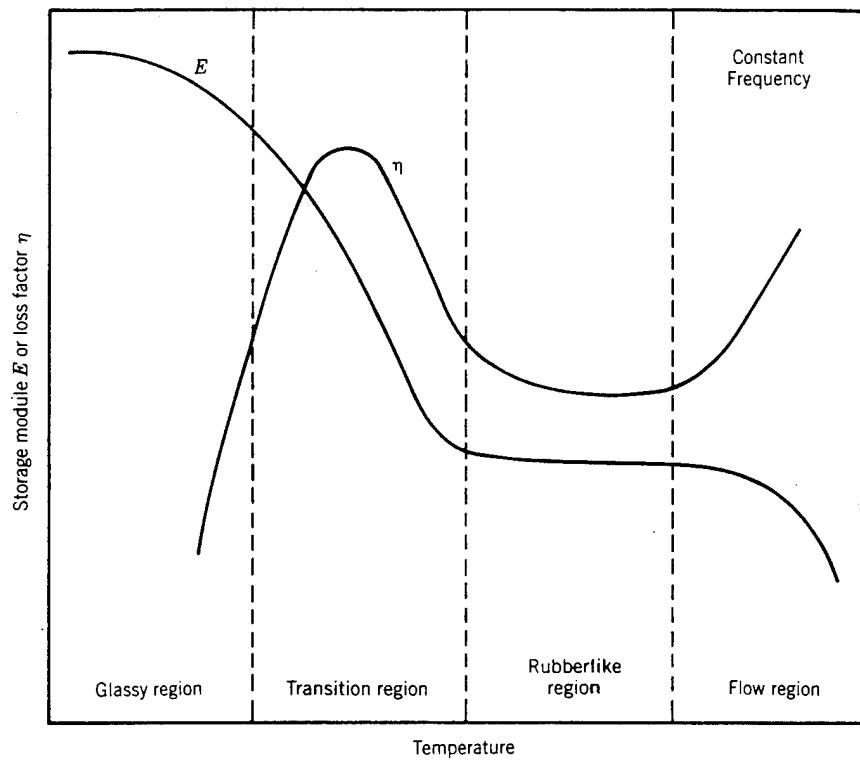
Temperature

Figure 2.1. Variation of Viscoelastic Material Properties with Temperature. [Ref. 6]

The effects of frequency on material properties are shown in Figure 2.2. The storage modulus always increases while the loss factor increases to a peak value in the transition region and starts to drop off as frequency enters the glassy region. It is important to realize that a temperature change of only a few degrees may have the same effect on material damping properties as a frequency change of several decades.

4
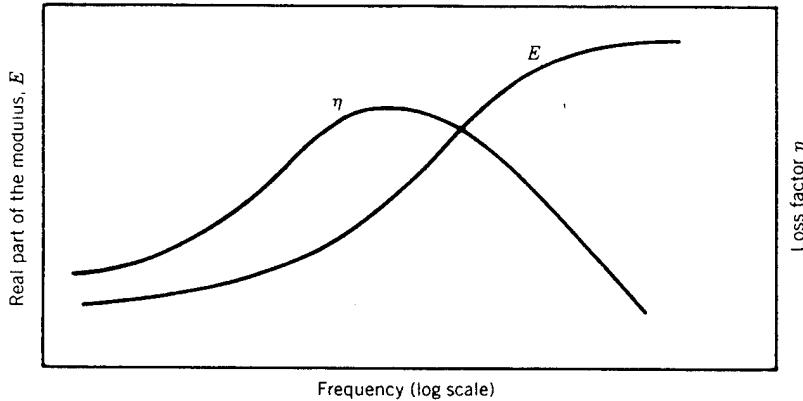
Figure 2.2. Variation of Viscoelastic Material Properties with Frequency at a Constant Temperature. [Ref. 6]

The effects of cyclic strain amplitude on the damping properties of viscoelastic materials are not easy to quantify. As the strain amplitude of a material increases, the energy dissipation of the material also increases resulting in a rise in material temperature. The trend follows the same general pattern as the temperature effects but to a smaller degree. This effect is illustrated in Figure 2.3.
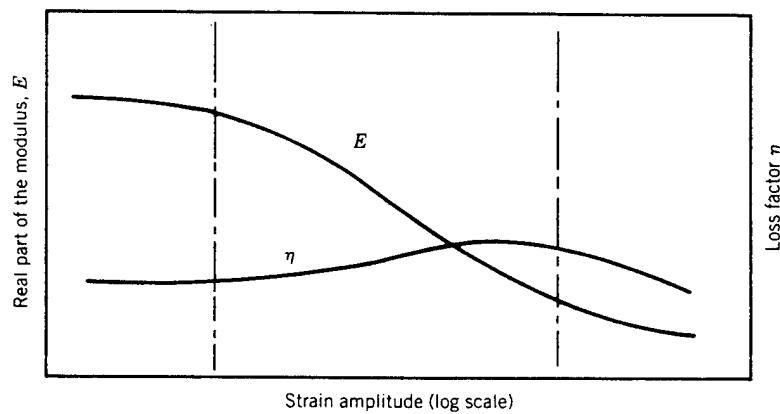

Figure 2.3. Variation in Viscoelastic Material Properties with Cyclic Strain Amplitude. [Ref. 6]

5

In order to accurately predict the effects of a viscoelastic damping treatment, one must take into account both temperature and frequency effects. Viscoelastic material property variations for commonly used materials are presented using a "reduced frequency nomogram". This plot shows the variation in the material loss factor and shear modulus as a function of both frequency and temperature. The viscoelastic material used in this work was 3M ISD-112 manufactured by the 3M Company. The associated nomogram is provided in Figure 2.4. In order to use this figure, simply enter the frequency of interest. Move horizontally to the left until the frequency intersects the diagonal constant temperature line. Move vertically up or down until the shear modulus or loss factor curve is intersected. Read the value of the desired material property from the respective scale on the left hand margin of the graph.
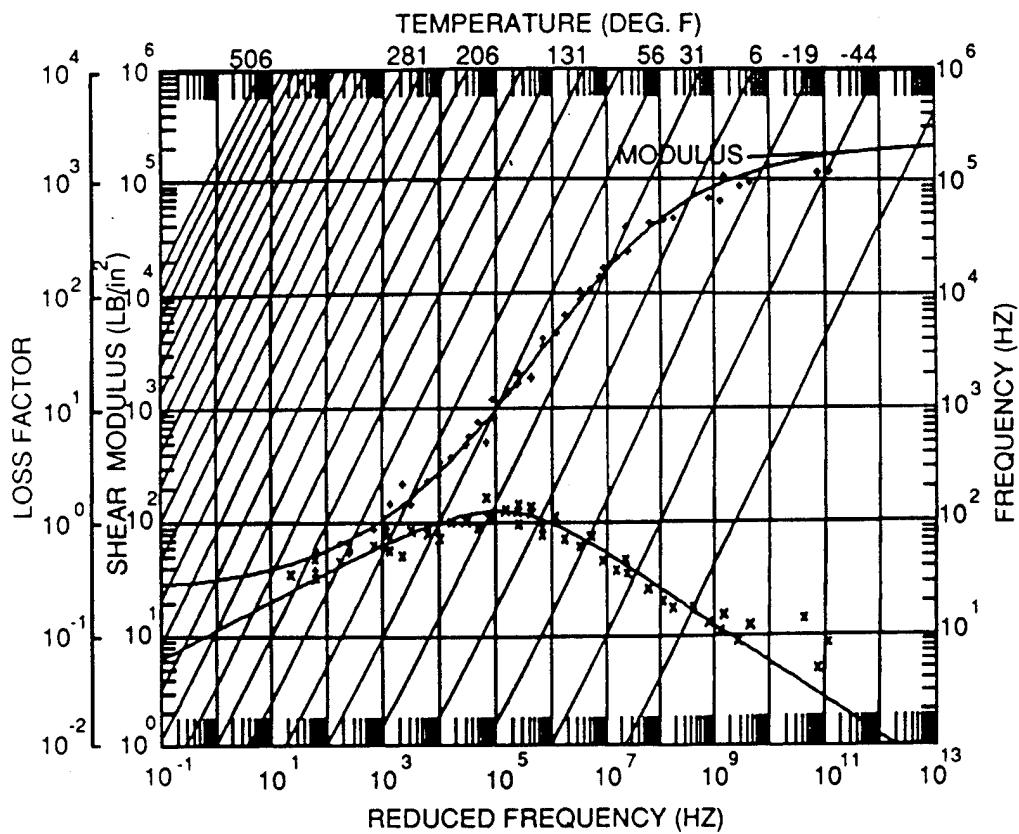

Figure 2.4. Reduced Frequency Nomogram for 3M ISD-112.

6

B.   STRUCTURAL DAMPING

The dynamic response of a structure is determined by the applied forcing function and three structure properties: mass, stiffness, and damping. Of these three damping is the hardest to predict. In most cases damping can only accurately be determined after conducting structural testing. Any system undergoing vibration will contain a kinetic energy component and a potential energy component. The kinetic energy is associated with mass and the potential energy is associated with stiffness. In addition, a vibrating structure will have an energy dissipation component known as damping.

All structures contain at least a small amount of damping as a result of the fabrication process. Any component on the structure that converts mechanical energy to thermal energy is a structural damping element. Examples include rivet joints, as well as, weld joints. The amount of system damping due to structural elements is usually very small and on the order of 1 to 2 percent. The damping level of a structure can be dramatically increased by the addition of a constrained viscoelastic layered damping treatment which will be discussed in more detail in later sections. Three primary effects of damping are (1) reduction of peak vibration amplitude at resonance; (2) slight lowering of the resonance frequency; (3) increased decay of the system dynamic transient response.

1.   Constrained Viscoelastic Layered Damping

A simple single constrained viscoelastic layered damping treatment is illustrated in Figure 2.5. It should be noted that Figure 2.5 is not drawn to scale.
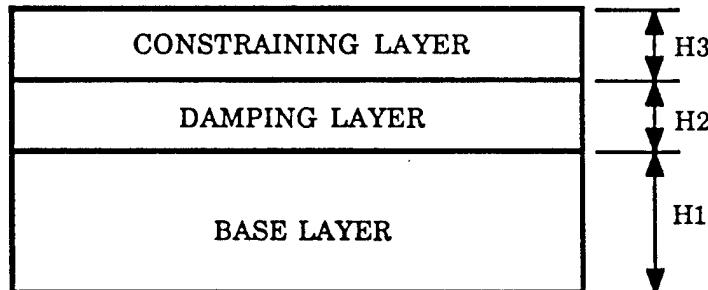

Figure 2.5. Simple Constrained Viscoelastic Layered Damping Treatment.

This configuration consists of the base layer (structure base), viscoelastic damping layer, and constraining layer. The stiffness of the top layer and base layer are usually much greater than the viscoelastic layer. As the system undergoes vibration, the base layer will deform and bend. This will cause the surface away from the composite body neutral axis to elongate stretching the viscoelastic layer. The top layer tends not to elongate due to its high stiffness thereby constraining the viscoelastic layer. Due to this constraining action during vibration, cyclic shearing strains are developed in the viscoelastic material. This shear strain energy is subsequently dissipated in the form of heat. For the constraining layer to be effective, its stiffness should not exceed that of the base layer [Ref. 7, 8].

In designing a damping treatment it must be determined whether the surface will have full or partial coverage. Partial coverage techniques are often used when weight savings is a concern. To effectively design a partial coverage scheme one must have knowledge of the system mode shapes over the frequency range of interest. Once the modes of interest are determined locations of negectible strain energy may be eliminated. For constrained viscoelastic layered damping where the bending of the composite produces not only bending and extensional strains in all three layers, but also shear strain, the location of the nodal points become extremely important [Ref. 9]. A nodal point on a structure is a point of zero modal extension as the structure vibrates at a system natural frequency. A good example of a nodal point would be the inflection point of a sine or cosine wave. The amount of shear produced in a viscoelastic layer is maximum at the nodal points. Once the nodal points and high strain energy points are isolated, the length of the damping strip has to be determined. As a first approximation, one should keep uninterrupted lengths of the constrained layer treatment greater than 60 percent of the flexure wavelength of the composite to obtain loss factors which are no less than 50 percent of that obtained with a fully covered surface [Ref. 9].

8

C. SYSTEM ISOLATION METHODS AND CHARACTERISTICS

A simple way to reduce the undesirable effects of component vibrations is to use a vibration isolation mount. This method basically involves inserting a resilient member in between the vibrating mass and the source of vibration. Vibration isolators can either be active or passive. The scope of this work is limited to passive isolators only. Figure 2.6 illustrates a simple passive isolation system.
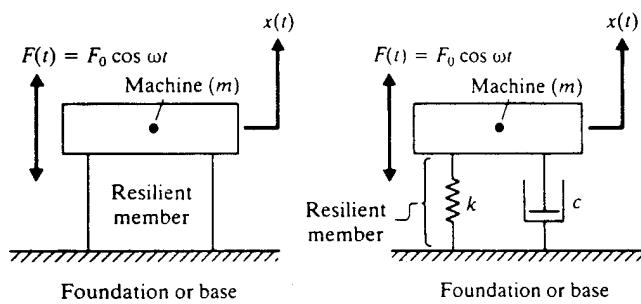

Figure 2.6. Simple Machine Isolator System. [Ref. 1]

The isolator is assumed to have both elasticity and damping which are modeled with a spring of stiffness k and a damper with damping coefficient c. The force developed by the rotating machine is assumed to be $F(t) = F_0 \cos (\omega t)$. The transmissibility or transmission ratio of the isolator, T, is defined as the ratio of the magnitude of the transmitted force to the excitation force. It can be shown that the transmissibility is given by [Ref. 1]:

$$T = \left[\frac{1 + (2\zeta \omega/\omega_n)^2}{[1 - (\omega/\omega_n)^2]^2 + (2\zeta \omega/\omega_n)^2} \right]^{1/2} \qquad (2.1)$$

9

where,

$$\omega_n = (k/m)^{1/2} \qquad (2.2)$$

$$\zeta = \frac{c}{2m\omega_n} \qquad (2.3)$$

Figure 2.7 shows the variation in transmissibility as a function of the forcing frequency to natural frequency ratio (ω/ω_n) for a simple passive isolator. It should be noted the isolation region does not begin until (ω/ω_n) is greater than 1.41.
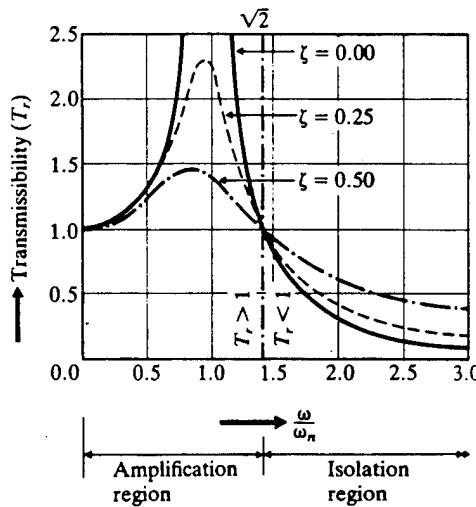

Figure 2.7. Variation of Transmission Ratio as a Function of (ω/ω_n). [Ref. 1]

D.   SYSTEM EQUATIONS OF MOTION

Several methods can be used to transform a continuous system into a discretized multidegree of freedom system. One such method involves approximating the distributed system mass with a finite number of elemental lumped masses. The elemental masses are then connected to each other by elastic and damping members. Linear and angular coordinates are then used to describe the motion of the lumped masses. The applied

10

forcing function is discretized to either a rotation or translation degree of freedom. The matrix equations of motion used to approximate the continuous system can now be written:

$$[M]\{\ddot{x}(t)\}+[C]\{\dot{x}(t)\}+[K]\{x(t)\}=\{F(t)\} \qquad (2.4)$$

where,

[M] = Mass Matrix

[K] = Stiffness Matrix

[C] = Damping Matrix

$\{x(t)\}$ = Displacement Vector

$\{F(t)\}$ = Applied Force Vector

Equation 2.4 represents a set of "n" coupled equations. Solving for the associated eigenvalues and using the principle of orthogonality allows these coupled equations to be written as a set of "n" uncoupled equations as follows [Ref. 4]:

$$\{\ddot{q}(t)\}+[\eta_i\omega_i]\{\dot{q}(t)\}+[\omega_i^2]\{q(t)\}=\{f(t)\} \qquad (2.5)$$

where,

$$\{x(t)\}=[\phi]\{q(t)\} \qquad (2.6)$$

$$\{f(t)\}=[\phi]^T\{F(t)\} \qquad (2.7)$$

$[\Phi]$ = Eigenvector Matrix

$\{q(t)\}$ = Modal Position Vector

$[\eta_i \, \omega_i]$ = Diagonal Modal Damping Matrix

$[\omega_i^2]$ = Diagonal Modal Frequency Matrix

η_i = Modal Loss Factor

$\{f(t)\}$ = Modal Force Vector

Each uncoupled equation of motion can now be solved independent and the total system response is determined simply by summing up each individual modal response.

III. ANALYTICAL TECHNIQUES AND RESULTS

A. OBJECTIVE

When designing a constrained viscoelastic layered damping treatment for a structure which utilizes partial coverage, the designer should have knowledge of the system mode shapes in the frequency range of interest. Knowledge of the strain energy distribution can also be beneficial. Modal testing of a structure provides the system natural frequencies as well as mode shapes but does not necessarily predict areas of high strain energy. As structures become more complex, the modal testing techniques will also become more complicated. In most cases a finite element method is the best course of action in determining detailed system response. This response can easily be validated with a limited modal testing scheme. In this thesis work, the *I-DEAS* finite element analysis (FEA) module was used to calculate system natural frequencies, mode shapes, modal strain, and modal strain energy distributions [Ref. 10].

B. TESTING STRUCTURE SELECTION

The focus of this work was to study structural dynamic response in the 0 to 100 Hz range. The goal was to obtain a structure which contained well defined complex (multiple side) mode shapes in this frequency range. After conducting some trial and error solutions using the *I-DEAS* FEA module on various structures, a final prototype was agreed upon and is illustrated in Figure 3.1.
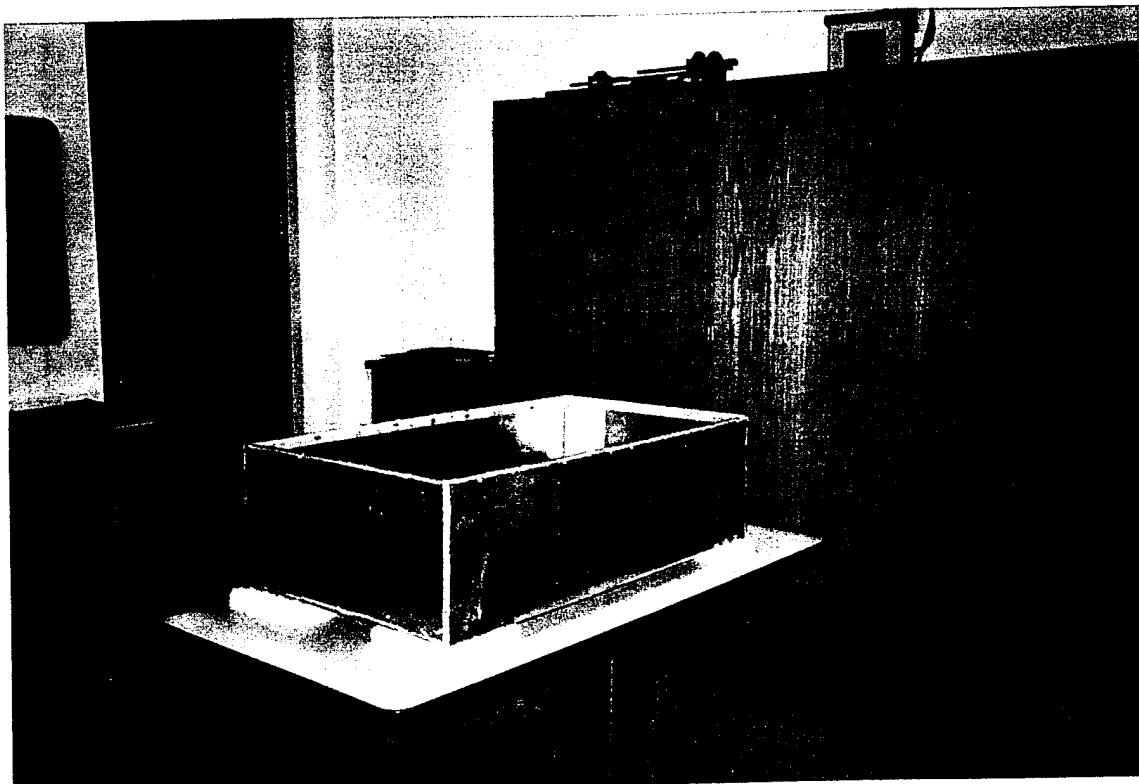
Figure 3.1. Testing Platform/System.

The structure is a long thin rectangular aluminum box with a wall thickness of 0.1 inches. The front and back face dimensions were 12 inches by 24 inches while the left and right sides were 12 inches by 42 inches. The top was left open for ease of experimentation. A finite element model was built in *I-DEAS* using 2600 elements and is provided in Figure 3.2.
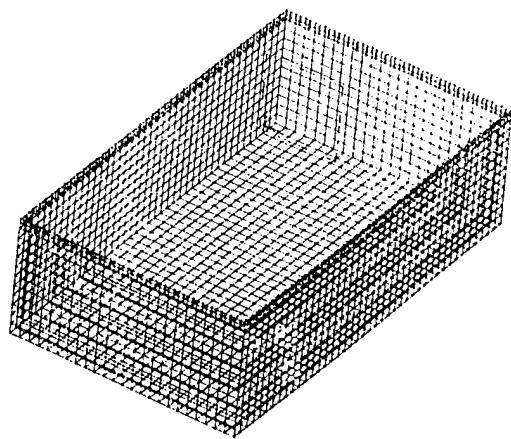

Figure 3.2. Finite Element Representation.

The structure was modeled as a free-free system to match the laboratory testing configuration. The system was modeled entirely with thin shell elements and beam elements. The beam elements were provided to simulate the stiffeners contained along the upper rim in the actual structure. It was known the testing platform would have a vibration generator with an associated support platform rigidly mounted to the base. Since the weight of this addition was not negectible to the total system weight, the added mass had to be taken into account in the finite element model.

Two approaches to the added mass were considered; one approach was to utilize the lumped mass option provided in *I-DEAS* and the other was to simply modify the density of a specific group of elements to account for the added mass. After analysis with both methods in *I-DEAS* the later option was chosen. The reason for this was because modifying the elemental densities better modeled the way the added mass was distributed.

C.   MODAL ANALYSIS RESULTS

The *I-DEAS* FEA module predicted twenty natural modes between 0 and 100 Hz (six rigid body and fourteen elastic) and are provided in Table 3.1. The associated modes shapes are provided in Figures 3.3 through 3.16. In addition to the normal modes, the *I-DEAS* FEA module was utilized to solve for the strain and strain energy distribution for each mode, which could be used in later analysis.

Table 3.1. *I-DEAS* **Predicted Natural Frequencies**

| MODE	FREQUENCY (Hz)	REMARKS
1-6	0	Rigid Body Modes
7	12.05	Torsional Mode
8	20.96	Breathing Mode
9	28.86	Breathing Mode
10	32.08	Left and Right sides in phase
11	42.02	Bottom side dominant
12	42.84	Left and Right sides in phase
13	51.35	All sides. Left / Right Sinusoid
14	58.29	All sides. Left / Right Sinusoid
15	62.07	Bottom side dominant
16	67.87	Right side Sinusoid. Front and Back out of phase.
17	72.46	All sides. Left / Right Sinusoid
18	72.91	All sides. Left / Right Sinusoid
19	85.78	All sides. Left / Right Sinusoid
20	93.9	Bottom side dominant. Left / Right in phase
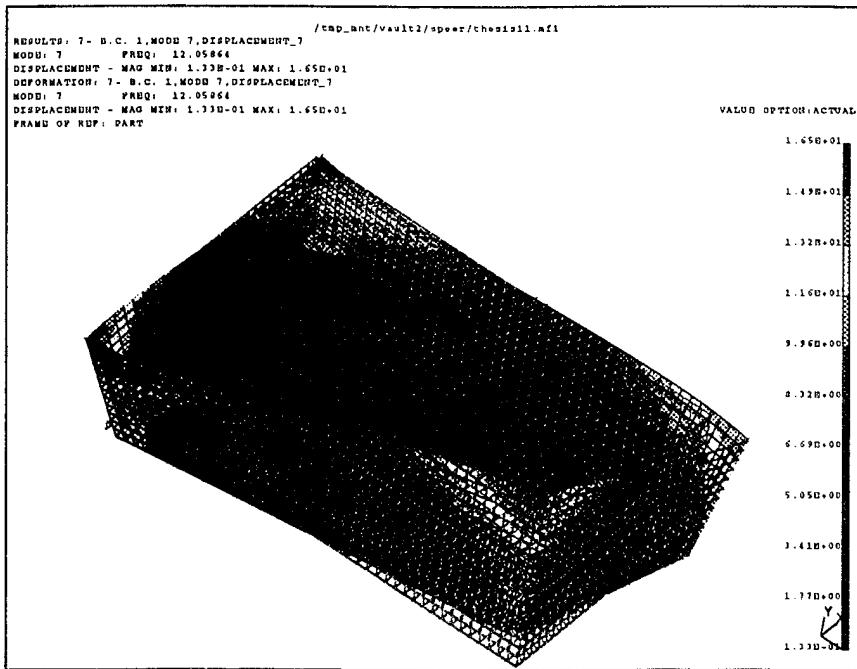
Figure 3.3.   12.05 Hz Mode Shape.
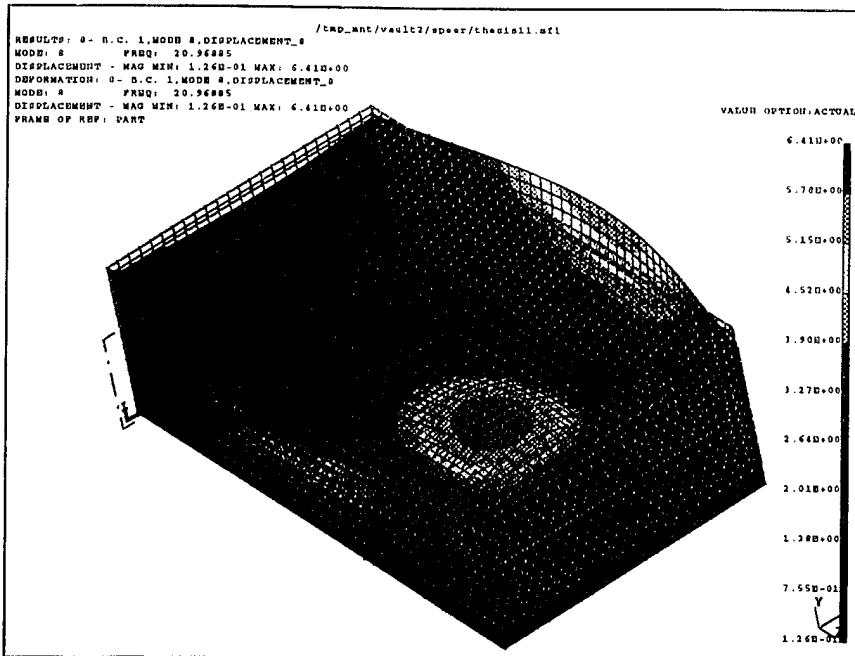

Figure 3.4.   20.96 Hz Mode Shape.

17
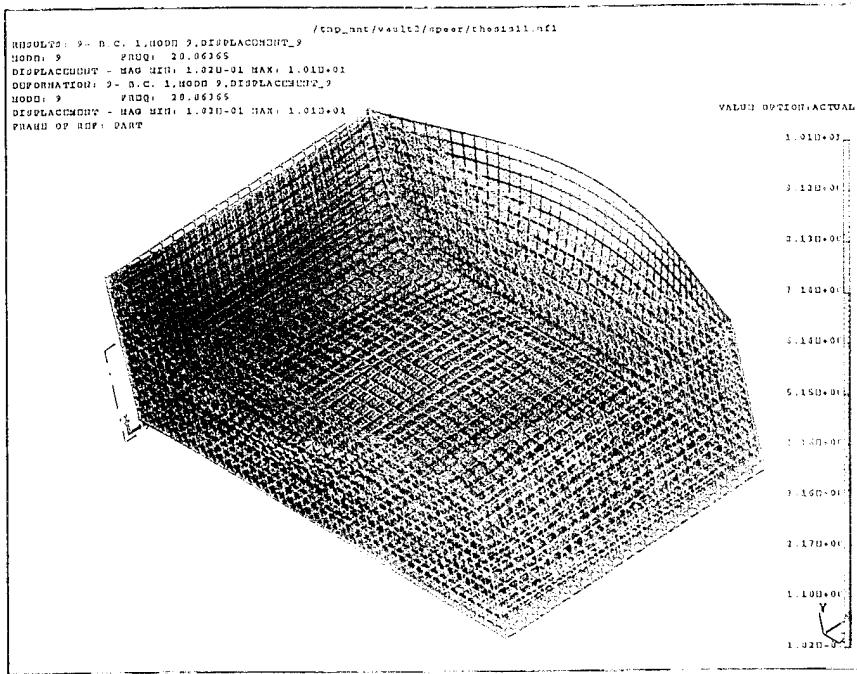
Figure 3.5. 28.86 Hz Mode Shape.
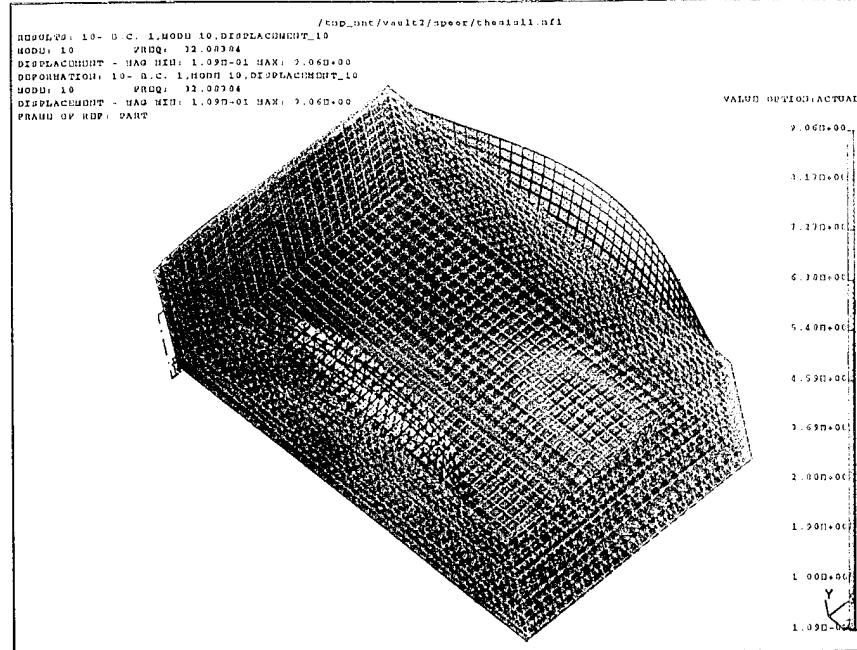

Figure 3.6. 32.08 Hz Mode Shape.

18
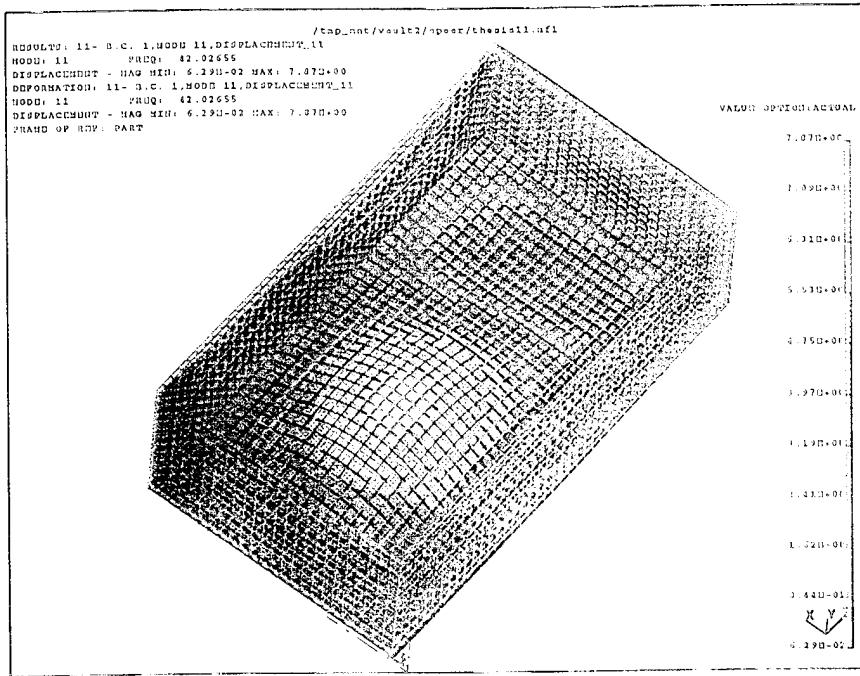
Figure 3.7. 42.02 Hz Mode Shape.
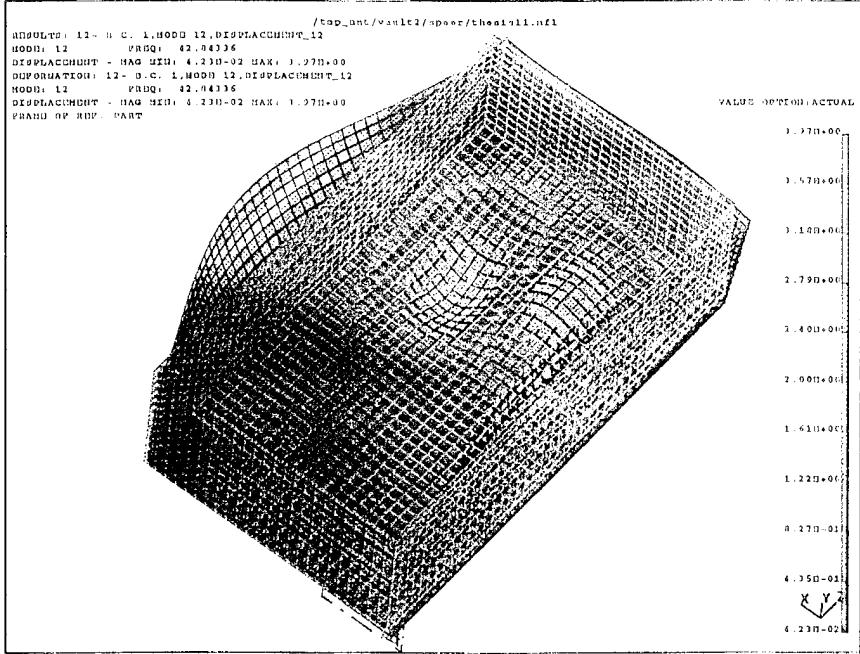
Figure 3.8. 42.84 Hz Mode Shape.

19
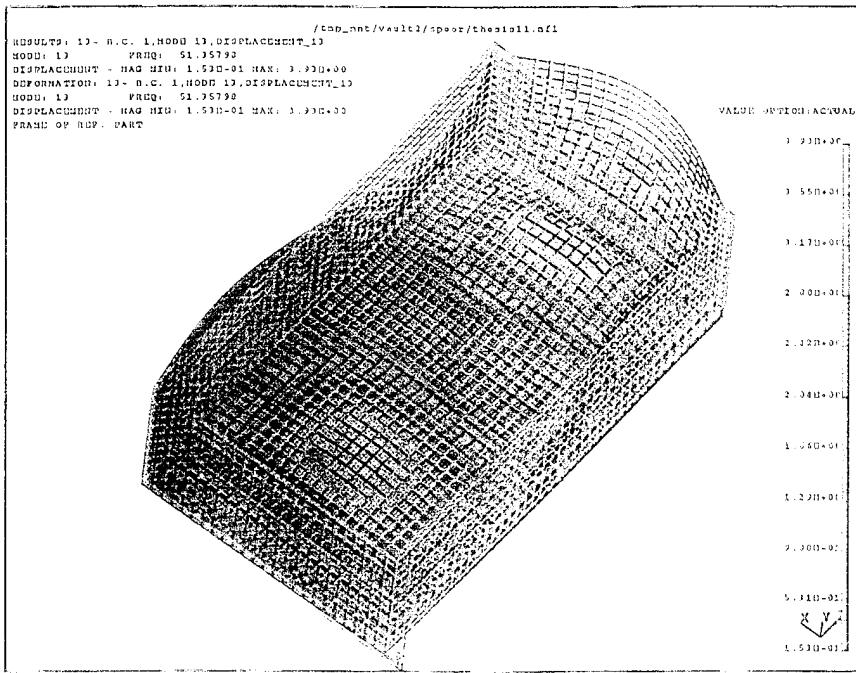
Figure 3.9.   51.35 Hz Mode Shape.
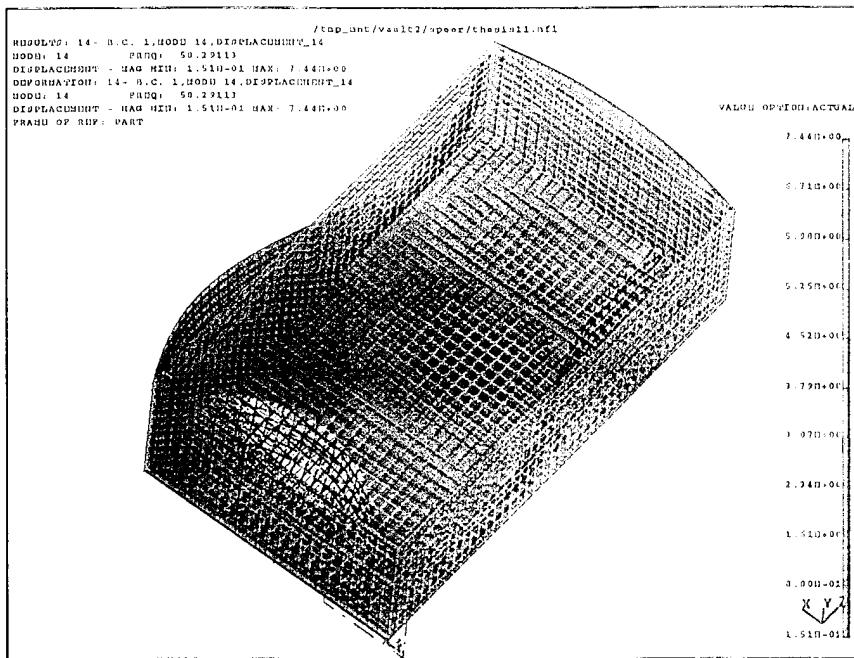
Figure 3.10.   58.29 Hz Mode Shape.

20
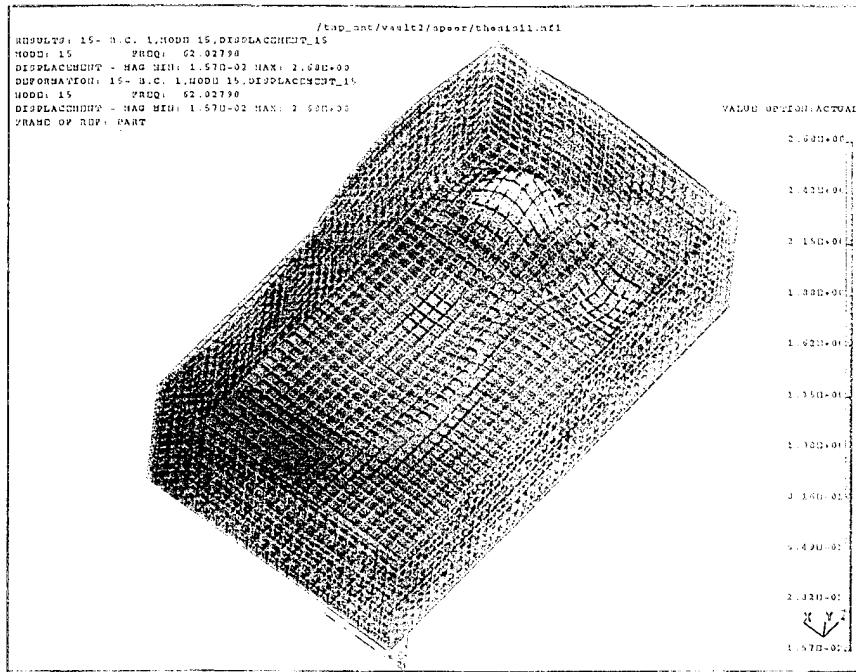
Figure 3.11. 62.02 Hz Mode Shape.
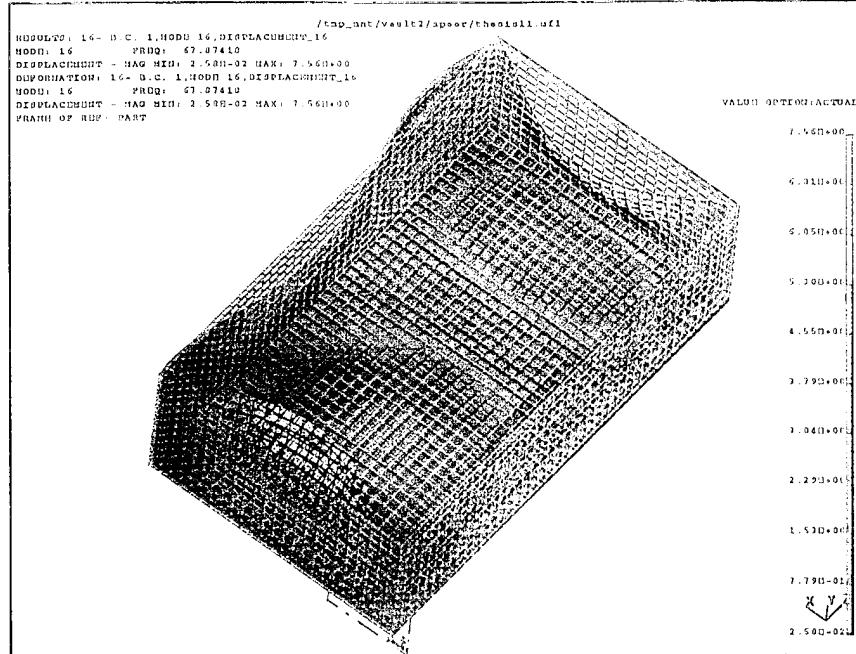

Figure 3.12. 67.87 Hz Mode Shape.

21
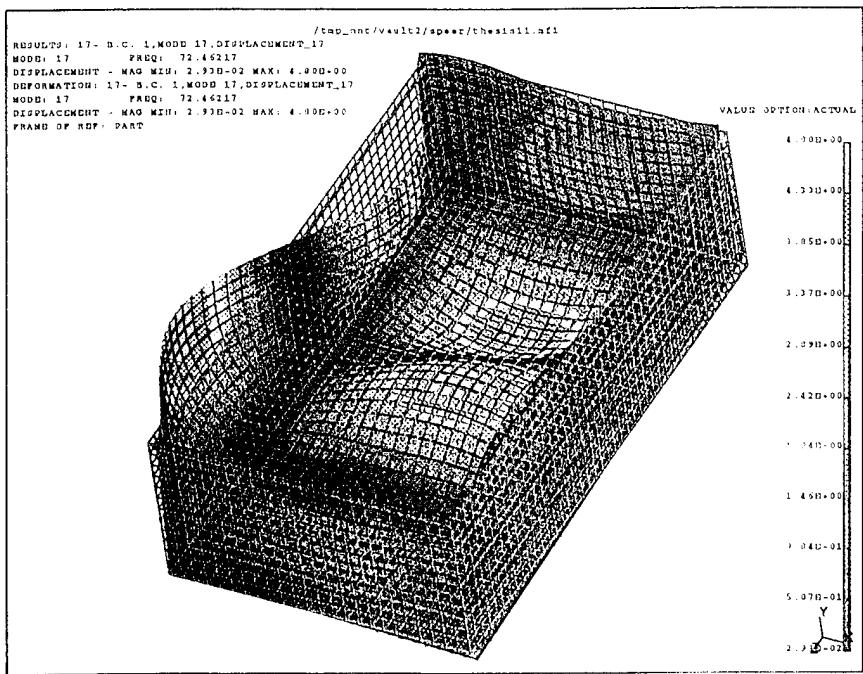
Figure 3.13. 72.46 Hz Mode Shape.
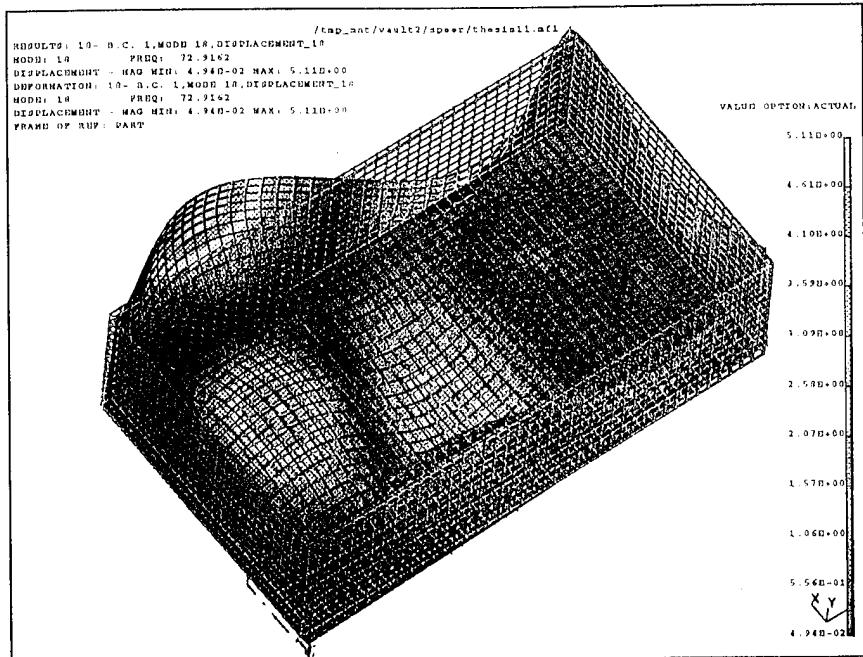
Figure 3.14. 72.91 Hz Mode Shape.

22
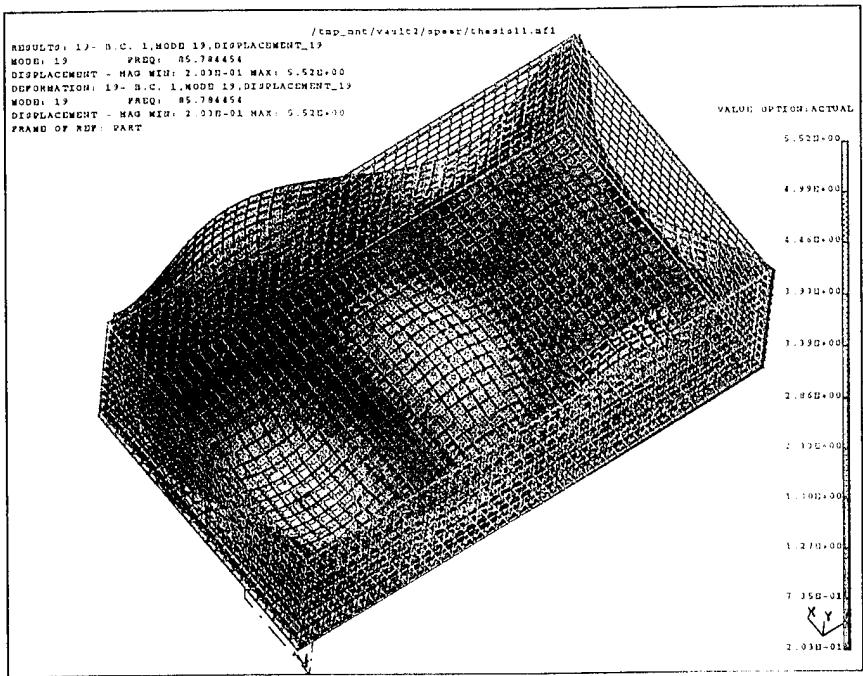
Figure 3.15.   85.78 Hz Mode Shape.
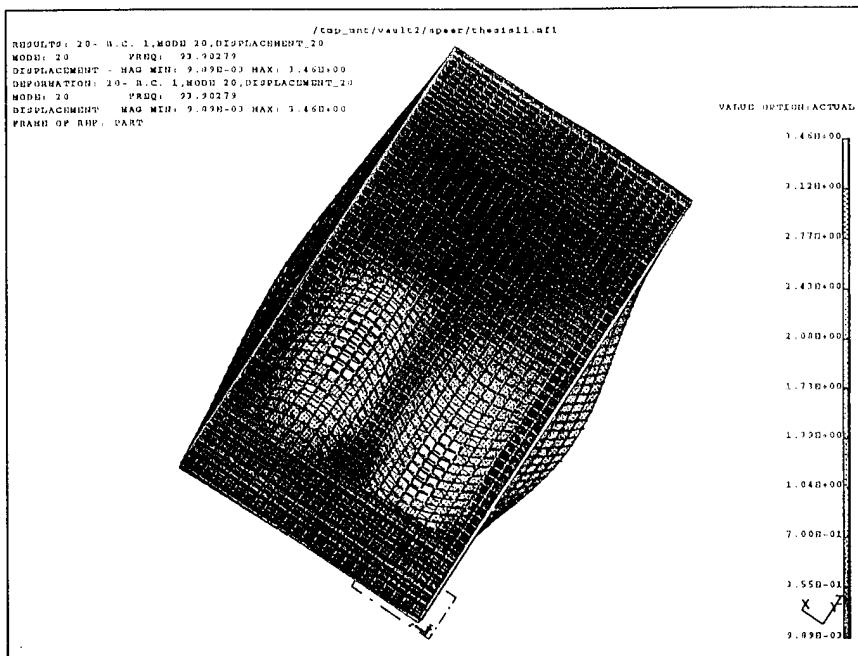
Figure 3.16.   93.9 Hz Mode Shape.

23

IV. DESIGN OF CONSTRAINED VISCOELASTIC LAYERED DAMPING TREATMENT

In order to approximate system loss factors and hence determine viscoelastic and constraining layer thickness required for maximum damping, an analysis based on the Ross-Kerwin-Ungar (RKU) equations was used [Ref. 11]. The equations are based on the analysis of a simple sandwich configuration shown in Figure 4.1.

```
+--------------------------------+   ┬
|     CONSTRAINING  LAYER        |   ⇕  H3
+--------------------------------+   ┴ ┬
|       DAMPING  LAYER           |     ⇕  H2
+--------------------------------+   ┬ ┴
|                                |   |
|         BASE  LAYER            |   H1
|                                |   |
+--------------------------------+   ┴
```
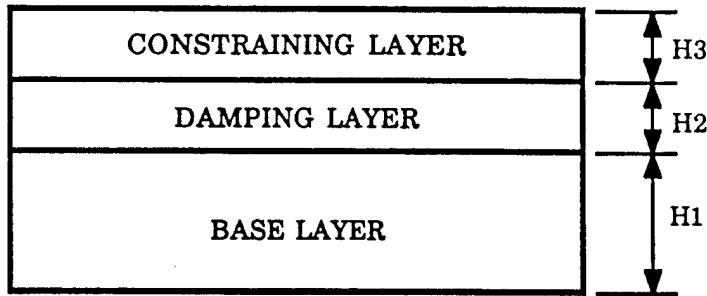
Figure 4.1. Elements of a Simple Sandwich Damping System.

The first step in determining the composite system loss factor is to determine the system flexural rigidity. The flexure rigidity, EI, of the above system can be written [Ref. 11]:

$$EI = \frac{E_1 H_1^3}{12} + \frac{E_2 H_2^3}{12} + E_1 H_1 D^2 + X - Y \qquad (4.1)$$

where,

$$X = E_2 H_2 (H_{21} - D)^2 + E_3 H_3 (H_{31} - D)^2 \qquad (4.2)$$

25

$$Y = \left[\frac{E_2 H_2^2}{12} + \frac{E_2 H_2}{2}(H_{21} - D) + E_3 H_3 (H_{31} - D) \right] \frac{H_{31} - D}{1 + g} \qquad (4.3)$$

$$D = \frac{E_2 H_2 \left(H_{21} - \frac{H_{31}}{2} \right) + g(E_2 H_2 H_{21} + E_3 H_3 H_{31})}{E_1 H_1 + \frac{E_2 H_2}{2} + g(E_1 H_1 + E_2 H_2 + E_3 H_3)} \qquad (4.4)$$

$$H_{31} = \frac{H_1 + H_3}{2} + H_2 \qquad (4.5)$$

$$H_{21} = \frac{H_1 + H_2}{2} \qquad (4.6)$$

$$g = \frac{G_2}{E_3 H_3 H_2 K^2} \qquad (4.7)$$

E = Young's Modulus

G = Shear Modulus

I = Moment of Inertia

H = Member Thickness

K^2 = Modal Wave Number

Subscripts refer to layers labeled in Figure 4.1. No subscripts implies composite system. For a plate on simple supports, the wave number is determined by [Ref. 11]:

26

$$K^2 = \frac{\omega_n}{\sqrt{\dfrac{EH^3 g_c}{12(1-v^2)H\rho}}}$$ (4.8)

where,

ω_n = Natural Frequency

g_c = Gravitational Constant

v = Poisson's Ratio of Composite Body

ρ = Density of Composite Body

To introduce damping into the equations, it is necessary to use the complex modulus concept discussed in reference 11. In order to reduce the analytical burden, the following assumptions were made:

(1) Damping of the base structure is small (i.e., $\eta_1 = 0$).

(2) Extensional stiffness of damping layer is small compared to rest of composite (i.e., $E_1 >> E_2$ and $E_3 >> E_2$).

(3) Damping of the constraining layer is small (i.e., $\eta_3 = 0$).

Under these assumptions the total system loss factor can be calculated using [Ref. 11]:

$$N_{sys} = \frac{\dfrac{12}{a^2+b^2}[A-B-C]_{IM}}{EH^3}$$ (4.9)

27

where,

$$EH^3 = E_1H_1^3 + E_1H_3^3 + \frac{12}{a^2+b^2}[A-B-C]_{RE} \qquad (4.10)$$

$$A = gE_1H_1E_3H_{31}^2[a+b\eta_2+i(\eta_2a)] \qquad (4.11)$$

$$B = E_1H_1E_2H_2H_{31}[a+b\eta_2+i(a\eta_2-b)] \qquad (4.12)$$

$$C = 2gE_2H_2E_3H_{21}H_{31}[a-\eta_2^2a+2b\eta_2+i(2a\eta_2-b+b\eta_2^2)] \qquad (4.13)$$

$$a = E_1H_1+g(E_1H_1+E_3H_3) \qquad (4.14)$$

$$b = g\eta_2(E_1H_1+E_3H_3) \qquad (4.15)$$

$$i = \sqrt{-1} \qquad (4.16)$$

η_2 = Viscoelastic Layer Loss Factor

IM = Imaginary Part

RE = Real Part

N_{sys} = System Loss Factor

28

These equations can now be easily programmed into a computer to estimate the loss factor for any configuration.

For the purpose of this experiment, each side of the structure was considered to be a flat plate. Since equation (4.8) was developed for a simply supported plate which did not match the testing configuration, the modal wave number was estimated by substituting the natural frequency for each mode calculated using the *I-DEAS* FEA Module.

There were two methods available for obtaining the viscoelastic layer loss factor and shear modulus. One was to read directly from the reduced frequency nomogram for a given temperature and frequency. A more advantageous method was to determine the loss factor and shear modulus using curve fit equations provided in reference 11. These equations, along with equations 4.1 through 4.16, were programmed into a MATLAB [Ref. 11], provided in Appendix A, to calculate loss factors for any configuration. Since viscoelastic material properties are frequency sensitive the solution had to be corrected for the final composite body natural frequency. This was accomplished by using an iterative loop program based on a procedure described in reference 11.

Figures 4.2 through 4.5 illustrate predicted system loss factors as a function of viscoelastic thickness, H_2, and constraining layer thickness, H_3, at four selected frequencies. All figures used a base thickness, H_1, of 0.1 inches.
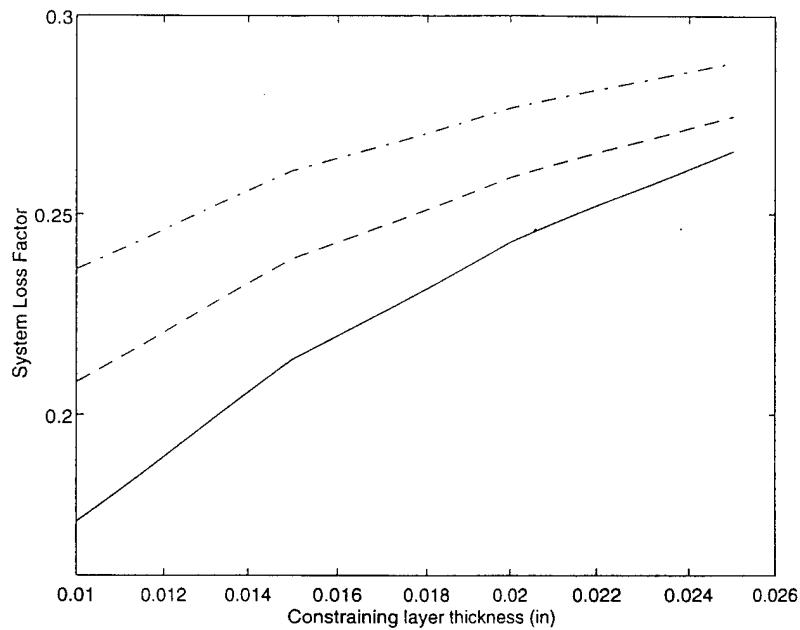
Figure 4.2. System Loss Factor as a function of H_2 and H_3 at 21 Hz.
[solid line: H_2 (0.025 inches) ; dash dot : H_2 (0.05 inches) ; dotted : H_2 (0.075 inches)]
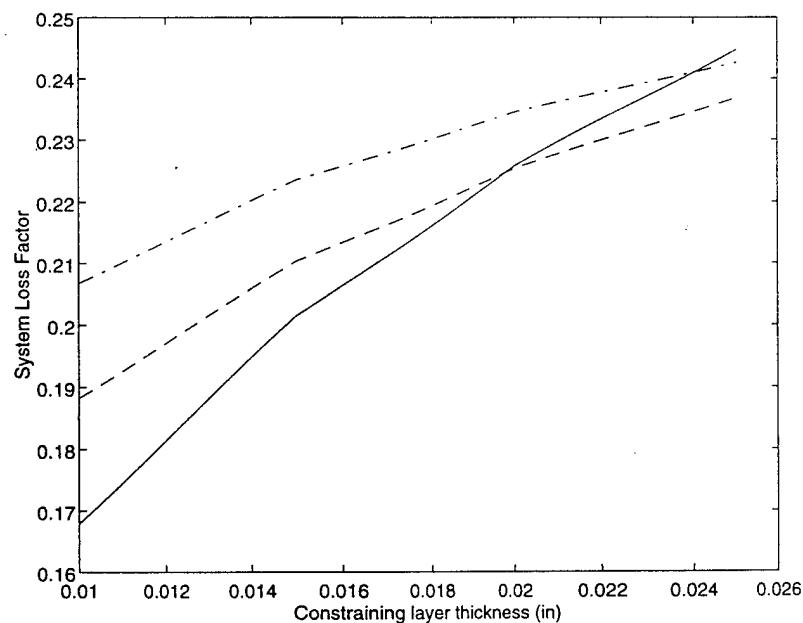
Figure 4.3. System Loss Factor as a function of H_2 and H_3 at 52 Hz.
[solid line : H_2 (0.025 inches) ; dash dot : H_2 (0.05 inches) ; dotted : H_2 (0.075 inches)]

30
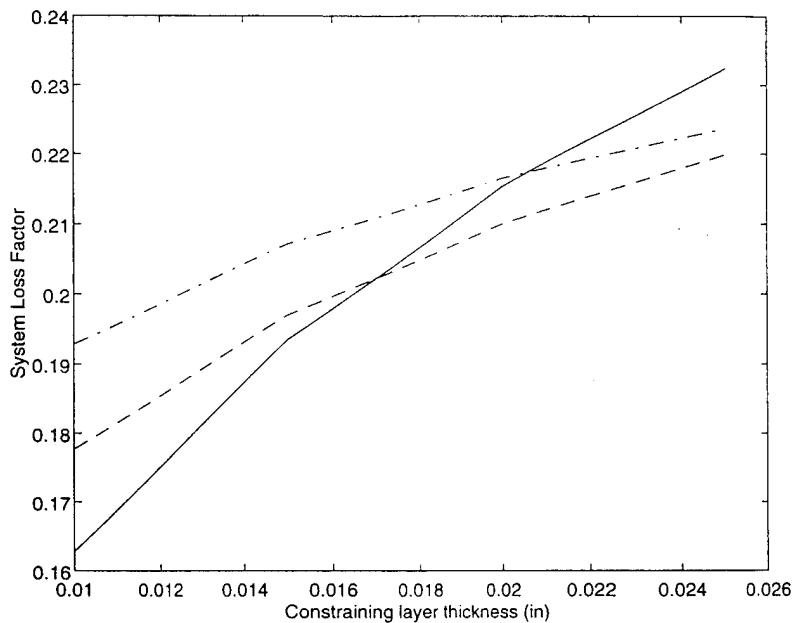
Figure 4.4. System Loss Factor as a function of H_2 and H_3 at 72 Hz.
[solid line : H_2 (0.025 inches) ; dash dot : H_2 (0.05 inches) ; dotted : H_2 (0.075 inches)]
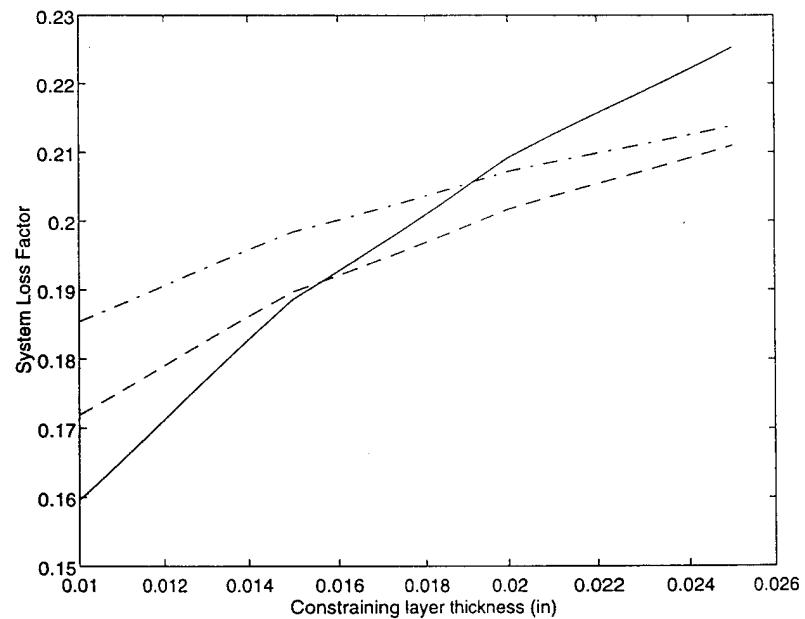

Figure 4.5. System Loss Factor as a function of H_2 and H_3 at 85 Hz.
[solid line : H_2 (0.025 inches) ; dash dot : H_2 (0.05 inches) ; dotted : H_2 (0.075 inches)]

31

It can easily be seen that as constraining layer thickness is increased the system loss factor increases. Surprisingly at some of the higher frequency iterations a viscoelastic layer thickness of 0.025 inches had a slightly higher loss factor than a thickness of 0.075 inches. In addition the maximum predicted loss factor decreased as frequency increased. After reviewing the predicted performance by the RKU equations and considering fabrication techniques it was decided to use the following configuration in laboratory testing:

$$H_1 = 0.1 \text{ inches (Base Structure)}$$
$$H_2 = 0.0390 \text{ inches (Viscoelastic Layer)}$$
$$H_3 = 0.025 \text{ inches (Constraining Layer)}$$

The predicted system loss factor as a function of frequency is provided in Figure 4.6.
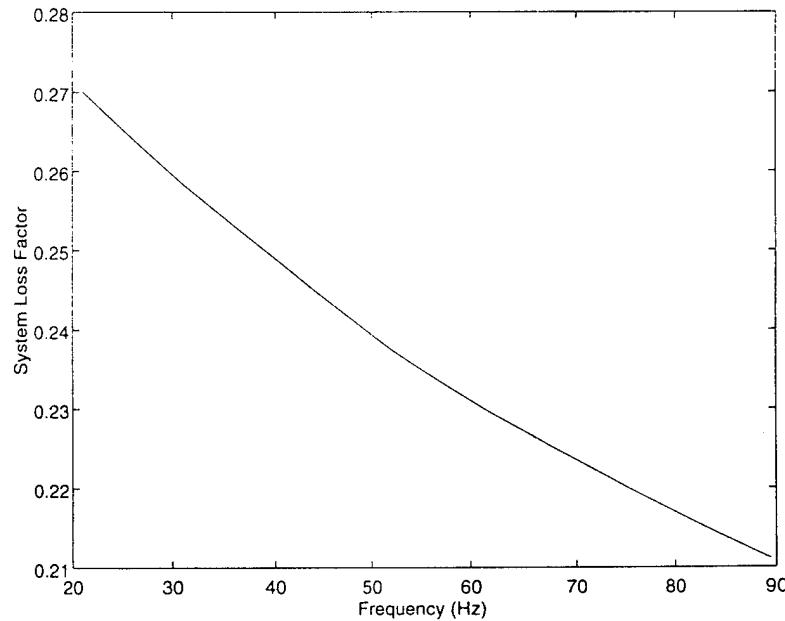
Figure 4.6. System Loss Factor as a Function of Frequency for Laboratory Configuration.

V. EXPERIMENTAL SETUP AND RESULTS

A.   TESTING ARRANGEMENT

Experimental testing was performed on the structure in three separate configurations:

(1) **Reference** structure without damping treatment.

(2) **Damped** structure using a constrained viscoelastic layered damping treatment.

(3) **Damped** structure with excitation source **isolated** with sound isolation mounts.

In order to approximate free-free boundary conditions, the structure was suspended from a wood frame with elastic cords, as shown in Figure 5.1.
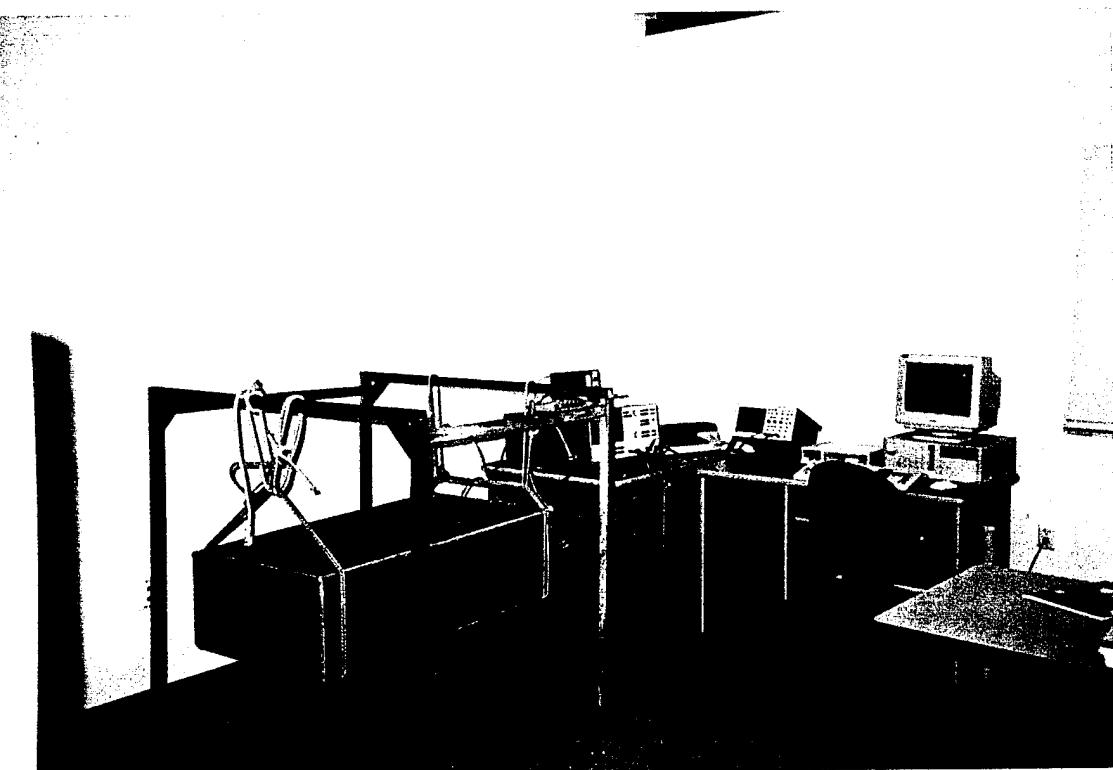
Figure 5.1. Structure Testing Configuration.

A 2 inch by 2 inch grid map was constructed on four sides of the testing structure to aid in the performance of the modal analysis. Figure 5.2 provides a representation of the testing platform with source placement. The bottom left hand corner of the structure was labeled as the origin for the experimental node numbering system. This allowed each point on the structure to have its own unique (x, y, z) coordinate for ease of data collection. For example all data collection locations on the left hand side were (0,y,z) and all points on the right side were (24,y,z).
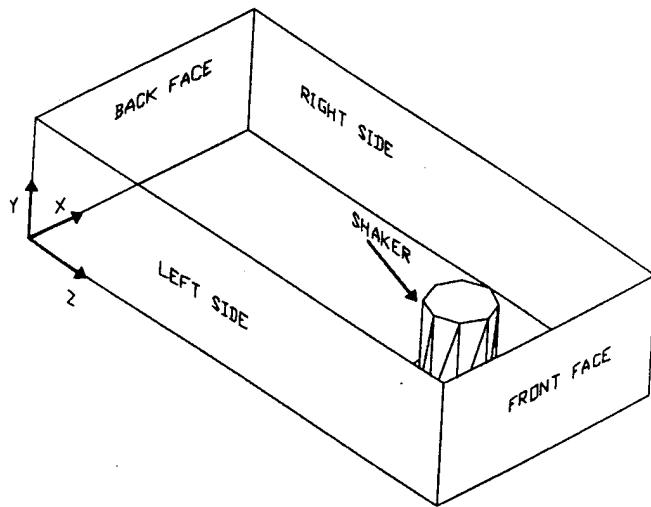
Figure 5.2. Testing Platform with Source Location.

The primary piece of testing equipment was the HP 3562A Dynamic Signal Analyzer (DSA) [Ref. 12]. The DSA was used to provide a swept sine signal to a vibration source generator, and to analyse the returning signals. The swept sine signal had a frequency range of 10 to 110 Hz. Ten averages were performed at each data point during the Frequency Response Function (FRF) survey using a frequency resolution of 125 mHz per step.

Figure 5.3 illustrates a block diagram of the testing scheme. The source signal was fed from the HP 3562A to a Wilcoxon Model F7/F4 Piezoelectric/Electromagnetic Vibration Generator (set a three volts) via a Wilcoxon PA7C power amplifier and a Wilcoxon impedance matching network [Ref. 13, 14]. The vibration generator was mounted on a 9 inch by 9 inch by 0.5 inch aluminum plate rigidly connected to the base of the testing structure located 4 inches from the front face and centered. An integral acceleration transducer mounted in the base of the vibration generator measured input acceleration and sent the signal into channel one of the DSA via a PCB model 462A charge amplifier. Structure acceleration was measured at various locations with an ENDEVCO model 2250A - 10 accelerometer. The acceleration signal was fed into channel two of the DSA via a PCB 483B07 model power supply. Frequency response data was measured and sent to a personal computer via the HPIB connection for storage and subsequent analysis. The raw data sent to the personal computer was a set of 1602 data points (both real and imaginary). A computer program was written to calculate the magnitude of the real and imaginary points and plot them as a function of the forcing frequency. A copy of this program is provided in Appendix B. Finally, a HP model 54601A four channel oscilloscope was connected to 3562A to monitor channel one and channel two signals. Figure 5.4 provides a photograph of the entire testing setup.
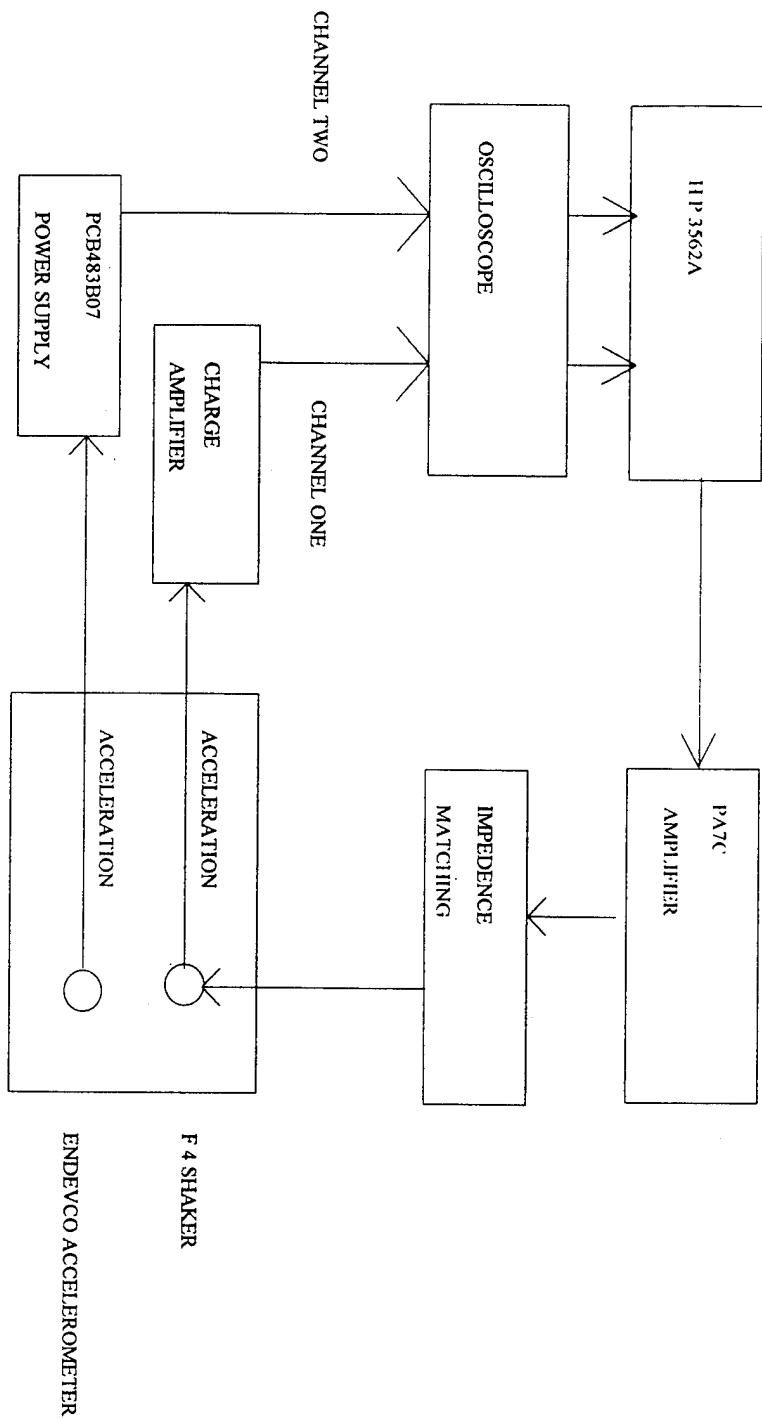
Figure 5.3. Testing Block Diagram.

36
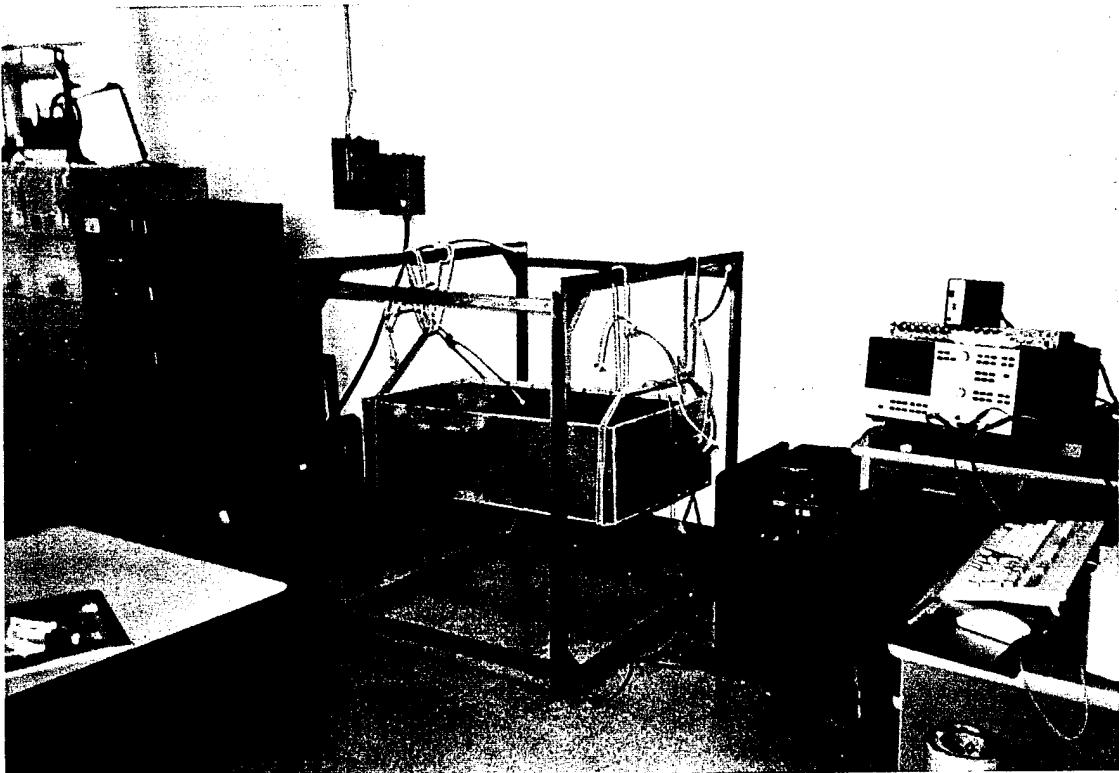
Figure 5.4. Testing Setup Photograph.

B. TEST OF THE SYSTEM WITHOUT DAMPING TREATMENT

The first part of the testing procedure was to perform a detailed frequency response analysis of the structure along the surface grid points. The purpose was to obtain the structure natural frequencies and mode shapes in the frequency range of interest. This data could then be compared to the *I-DEAS* FEA Module data to verify the *I-DEAS* model. The process involved acquiring FRFs at over 120 different locations. After reviewing the initial frequency response data, fifteen data point locations were chosen as the points where damping and isolation response data would be taken for comparison purposes. These points are listed as A - O in Table 5.1. Figures 5.5 through 5.7 illustrates examples of FRFs obtained.

37

Table 5.1. Key Data Collection Points

| Point	Coordinate (X,Y,Z)	Location
A	(0,10,20)	Left Side
B	(0,10,28)	Left Side
C	(0,8,12)	Left Side
D	(0,8,24)	Left Side
E	(0,6,24)	Left Side
F	(24,10,20)	Right Side
G	(24,6,12)	Right Side
H	(24,6,28)	Right Side
I	(6,10,42)	Front Face
J	(14,10,42)	Front Face
K	(14,6,42)	Front Face
L	(10,10,0)	Back Face
M	(10,6,0)	Back Face
N	(20,0,10)	Bottom
O	(4,0,20)	Bottom
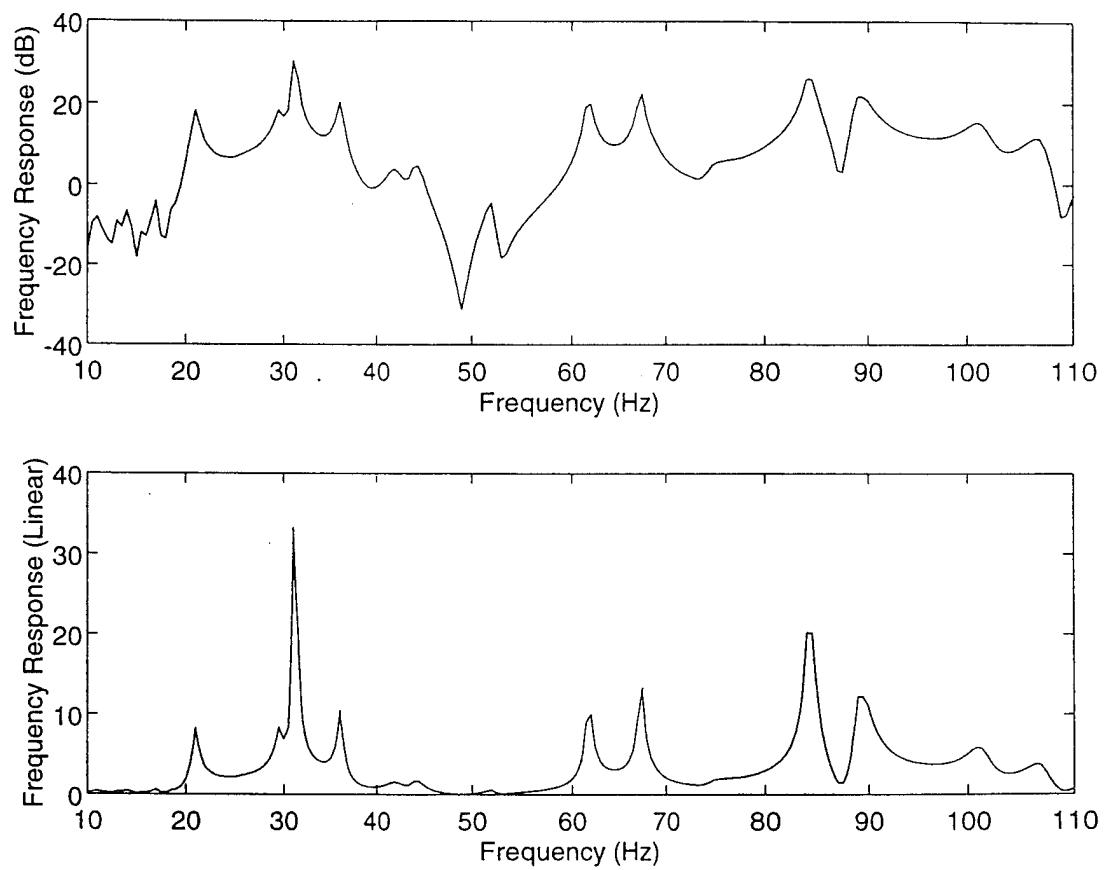
Figure 5.5. Reference Frequency Response: Testing Point E [Left Side ; (0,6,24)].
(*top* : dB scale ; *bottom* : Linear scale)
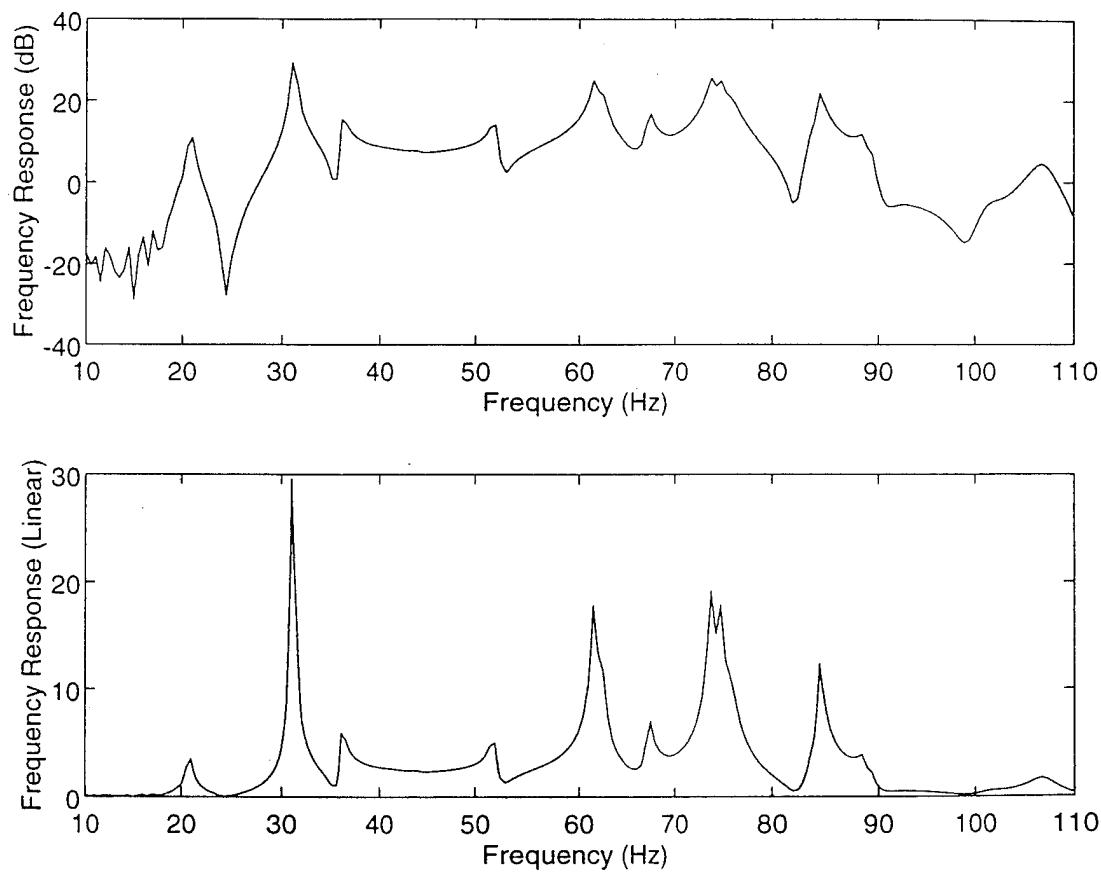
Figure 5.6. Reference Frequency Response: Testing Point K [Front Face ; (14,6,42)].
(*top* : dB scale ; *bottom* : Linear scale)
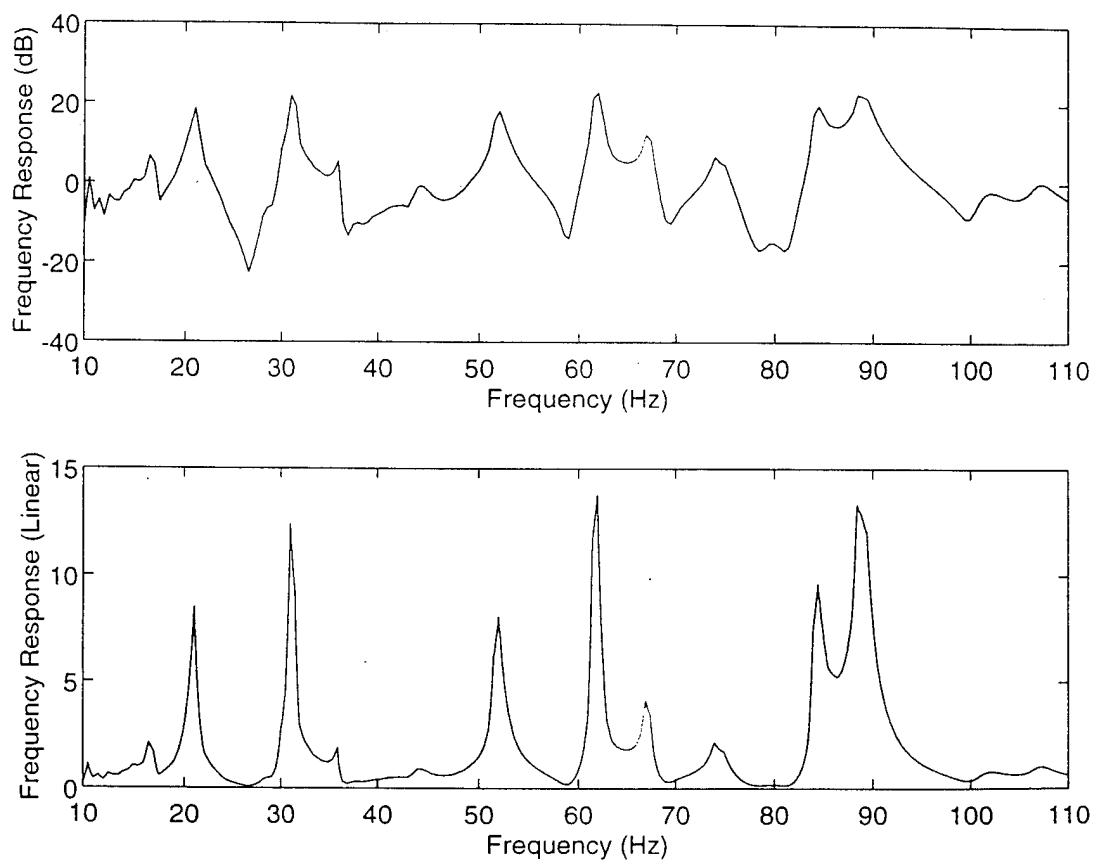
Figure 5.7. Reference Frequency Response: Testing Point N [Bottom ; (20,0,10)].
(*top* : dB scale ; *bottom* : Linear scale)

41

After completing this detailed analysis, twelve natural frequencies were isolated between 10 and 100 Hz. In addition to obtaining the natural frequencies, approximate mode shapes were determined for each natural frequency. This was accomplished by creating MATLAB contour plots derived from the response data. Figure 5.8 provides an example of an experimentally determined mode shape.
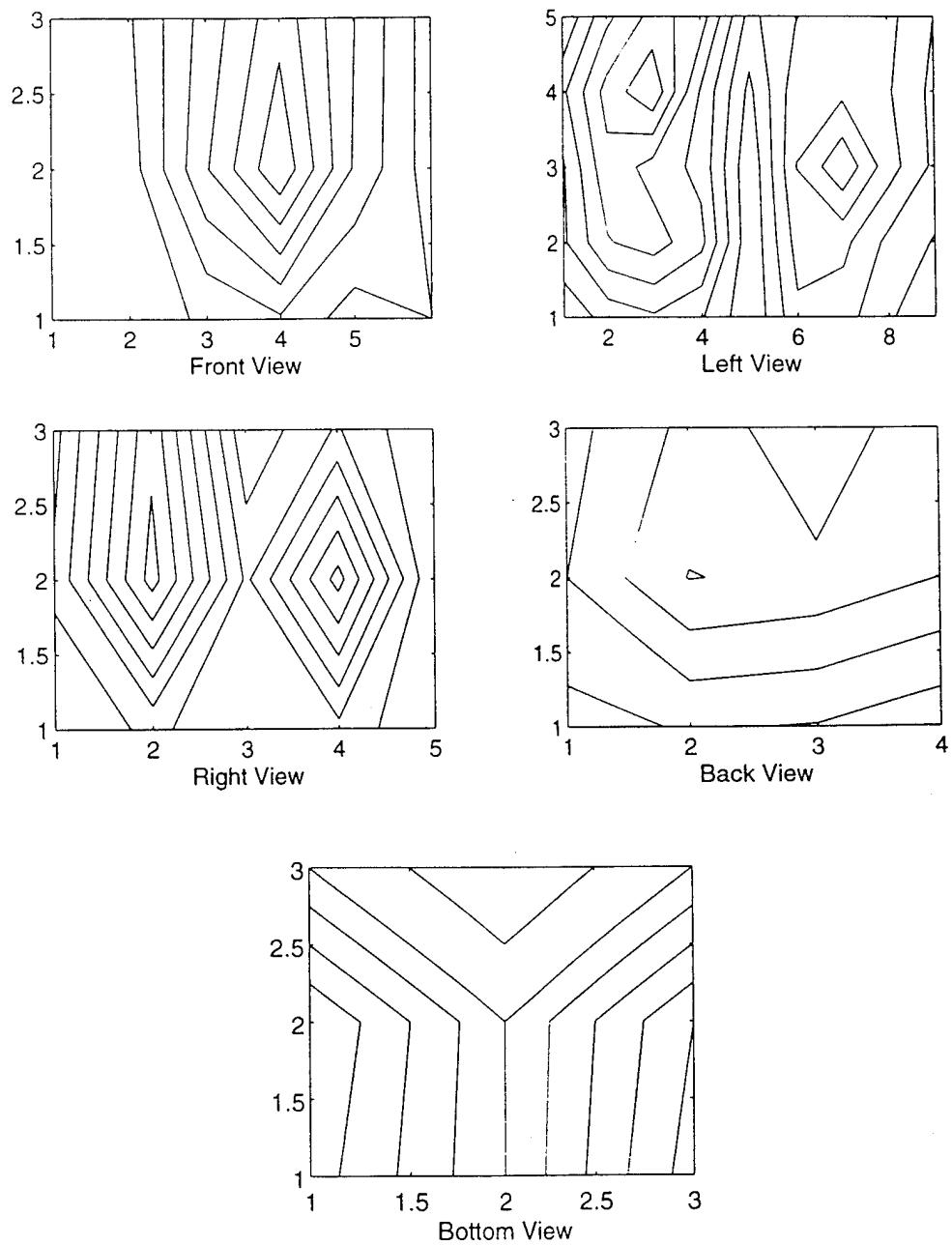
Figure 5.8. Experimental Mode Shape: 84 Hz.

The measured natural frequencies along with mode shapes were compared with analysis results to determine correlation between the two. Table 5.2 lists the experimentally determined natural frequencies along with the correlated analysis results.

Table 5.2. Experimental vs Analysis Modal Frequencies (Hz).

Experiment	Analysis	Percent Error (%)
21	20.96	0.19
31	28.86	6.9
36	32.08	10.88
44	42.02 / 42.84	2.64 (Note 1)
52	51.35	1.25
62	58.29	5.98
63	62.02	4.7
67.5	67.87	0.55
74	72.46	2.08
75	72.9	2.8
84	85.7	2.02
89.5	93.9	4.9

Note 1: Unable to distinguish between 42.84 and 42.02 Hz.

With the exception of three frequencies the percent error between experimental and analysis data was less than five percent.

Using a half power method calculation, initial structural damping was calculated for each mode to be used for comparison purposes in later experiments. Figure 5.9 provides a plot of percent structural damping as a function of natural frequency.
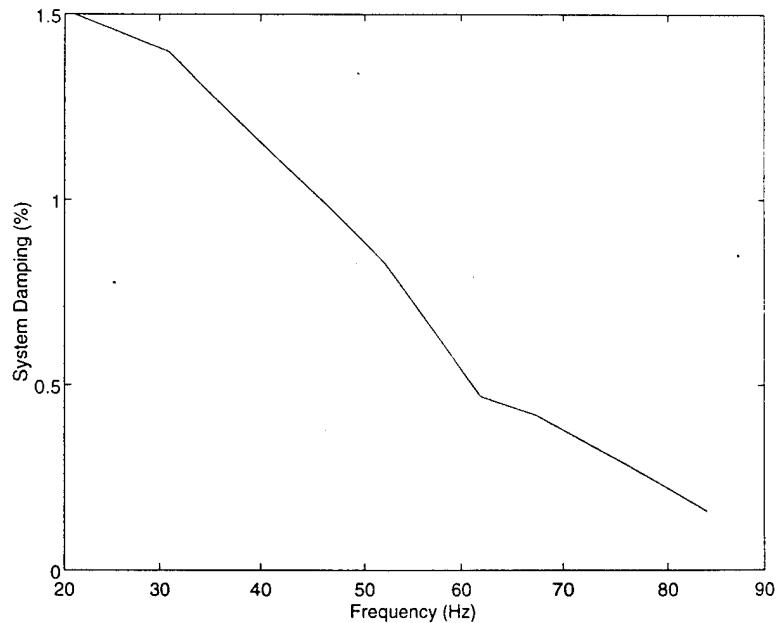

Figure 5.9. Percent Structural Damping as a Function of Natural Frequency.

C. CONSTRAINED VISCOELASTIC LAYERED DAMPING TREATMENT RESULTS

The constrained viscoelastic layered damping scheme discussed in earlier sections was applied to the structure in a partial coverage fashion. Three 9 inch by 9 inch strips were applied to both the left and right side (midspan and both quarter span locations) of the structure. The two quarter span locations represented areas of high extensional strain energy for most modes while the midspan was a nodal point for most of the higher frequencies. Two damping strips (12 inch by 5 inch and 12 inch by 4 inch) were applied to the front and back face in the midspan regions. These locations again represented areas of high extensional strain energy for most modes. In addition, a 15 inch by 16 inch strip was laid along the bottom section of the structure four inches from the back face and centered. Figures 5.10 illustrates a schematic of the damping scheme, while Figure 5.11 provides an actual photograph.

Left and Right Side Damping Locations

42

9x9   9x9   9x9

12
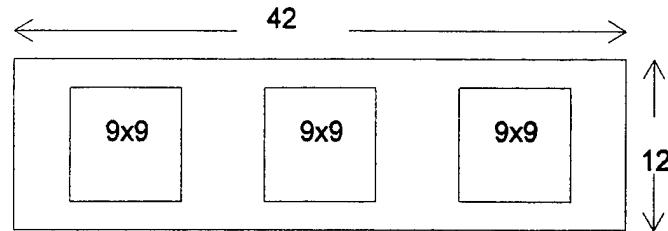
Bottom Face Damping Location

42

15x16

Source

24
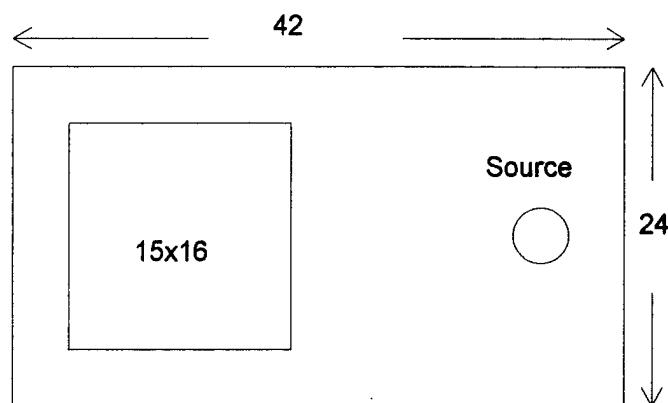
Front/Back Face Damping Locations

24

12x5

12x4

12
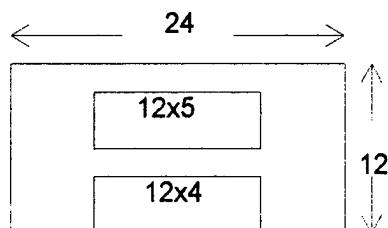
All Dimensions in inches

Figure 5.10. Damping Treatment Configuration.
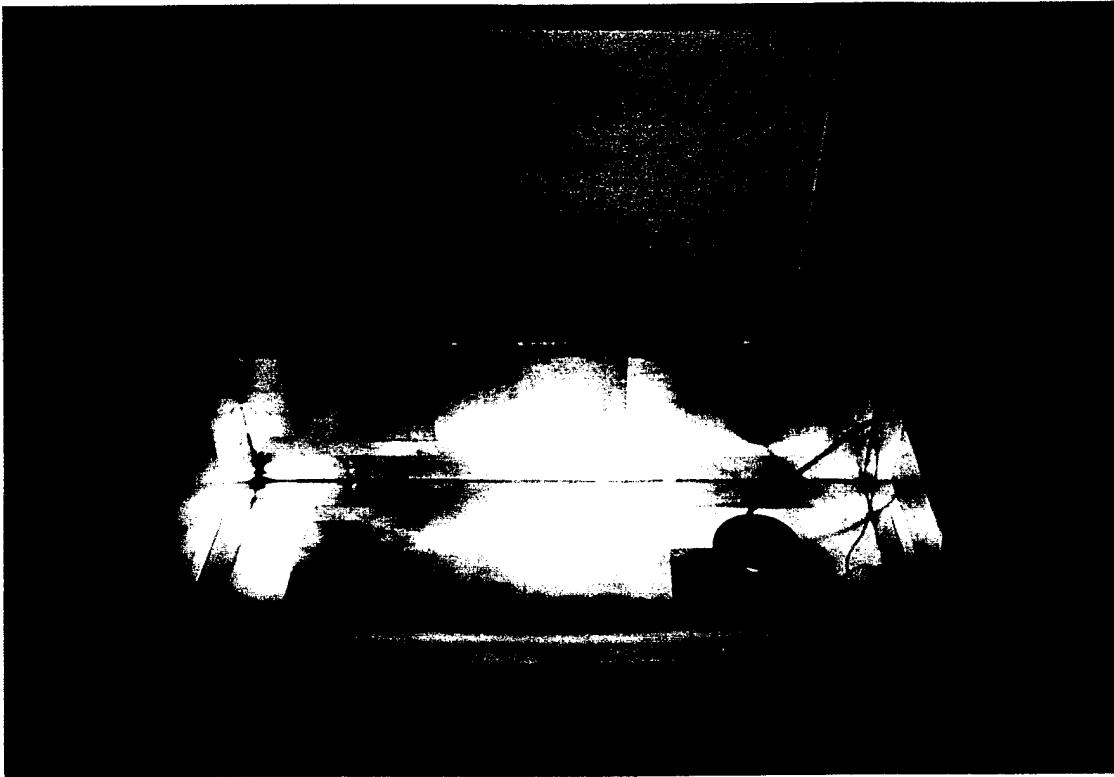
Figure 5.11. Damping Treatment Photograph.

Frequency response measurements were performed at points A - O to determine the average effectiveness of the damping material. As expected, the experimental loss factors were much less than predicted by the RKU equations. The system loss factors ranged from 0.03 to 0.0734. There are several reasons the experimental data does not match the predicted values. Examples include:

(1) RKU equations were based on a flat plate with simple supports. Experimental boundary conditions were much more complex.

(2) RKU equations assume full coverage of the damping material. A partial coverage technique was used.

Despite these variations the damping experiment was a success. The system damping in the constrained viscoelastic layered configuration varied from about 1.6 % at the lower frequencies to 3.7% at the higher frequencies. This represents an average increase of 14% at the lower modes and a 700% increase at the higher modes. Figure 5.12 illustrates the variation in damping as a function of frequency for the structure with and without the damping treatment. Due to coupling of modes, loss factors for all resonant points could not be calculated.
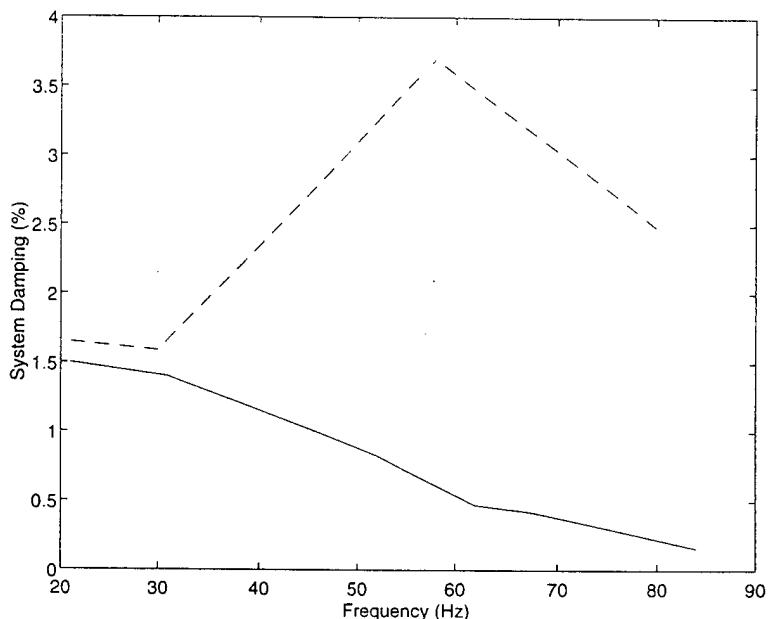
Figure 5.12. Percent Damping as a Function of Frequency.
[solid line: structure without damping treatment; dotted: structure with damping treatment]

The frequency response of the damped platform is characterized by a frequency shift to the left and a smoothing of the resonant points when compared to the reference structure. Additionally, there is a noticeable reduction in amplitude of resonant points over the frequency spectrum. In general, the reduction was greater in the higher frequency range of measurement. The 20 to 50 Hz range experienced a reduction of about 6 decibels (2: 1) while the 50 to 80 Hz range experienced a 20 decibel (10: 1)

the 80 to 100 Hz range experienced a 15.6 decibel (6: 1) reduction. Representative damped frequency response curves plotted together with the reference curves are shown in Figures 5.13 through 5.17.

——— structure without damping treatment

– – – – structure with damping treatment
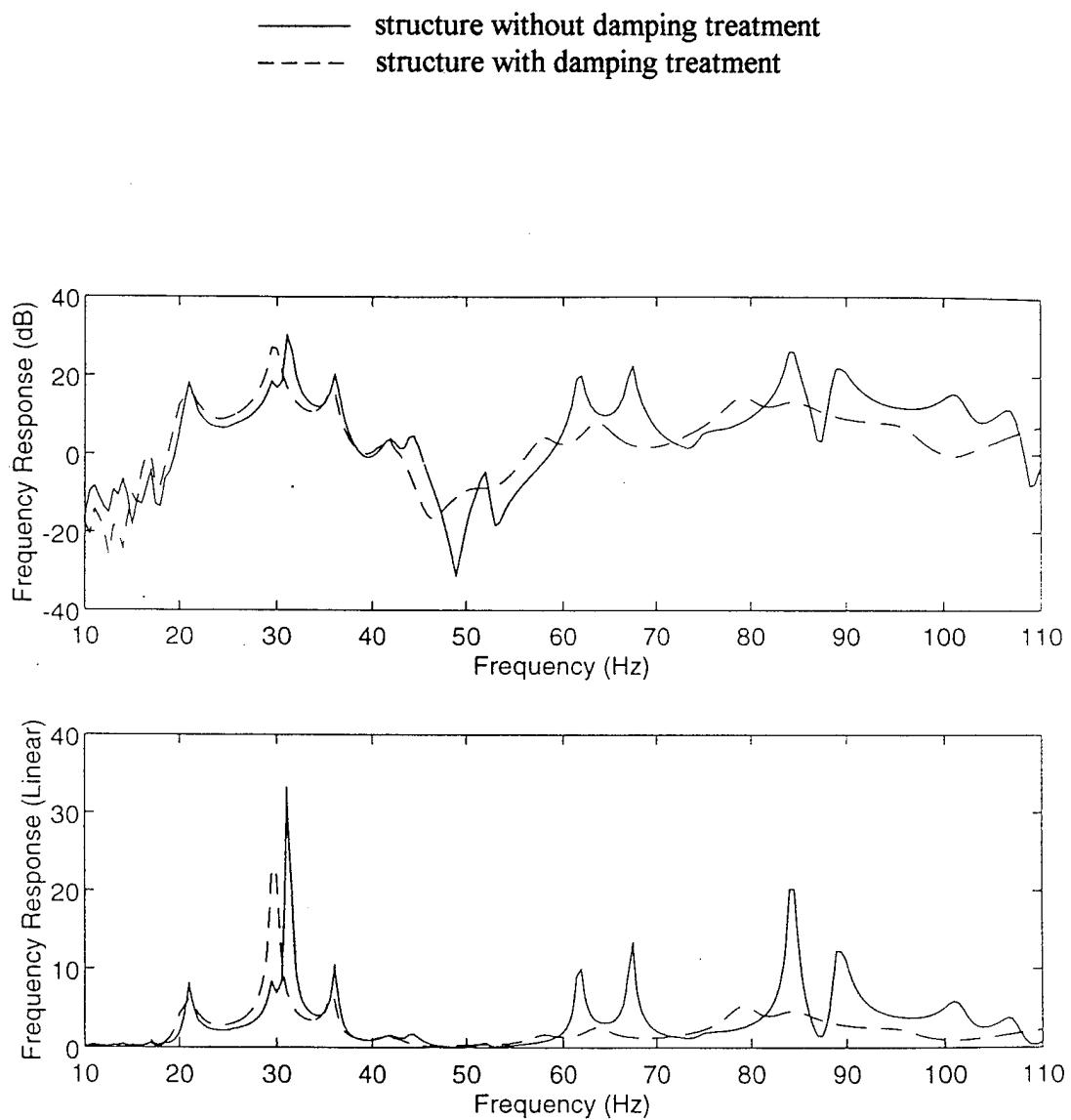
Figure 5.13. Frequency Response: Point E [Left side; (0, 6,24)].
(*top* : dB scale : *bottom* : Linear scale)

structure without damping treatment
- - - - structure with damping treatment
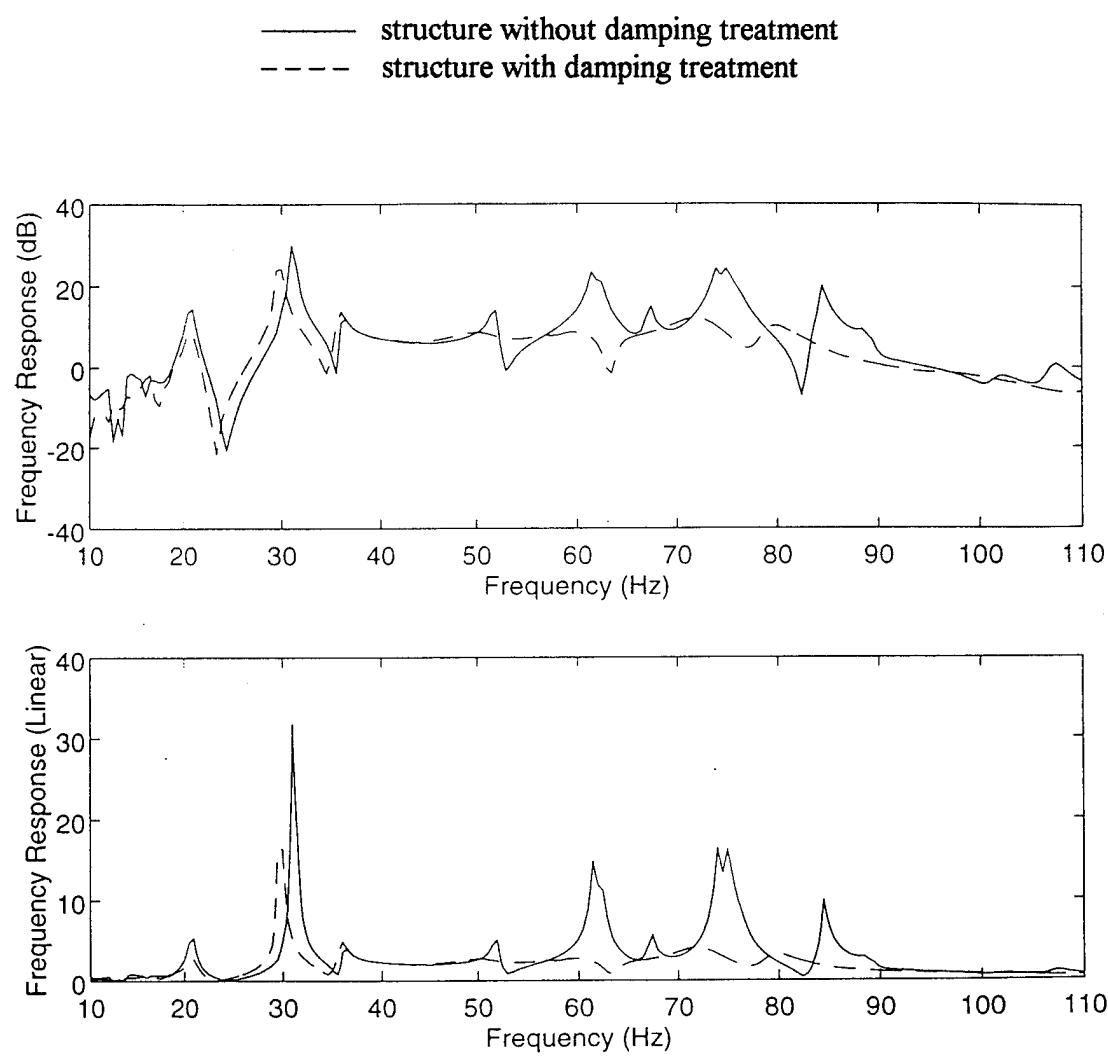
Figure 5.14. Frequency Response: Point J[Front face; (14, 10, 42)].
(*top*: dB scale; *bottom*: Linear scale)

50

————— structure without damping treatment

– – – – structure with damping treatment
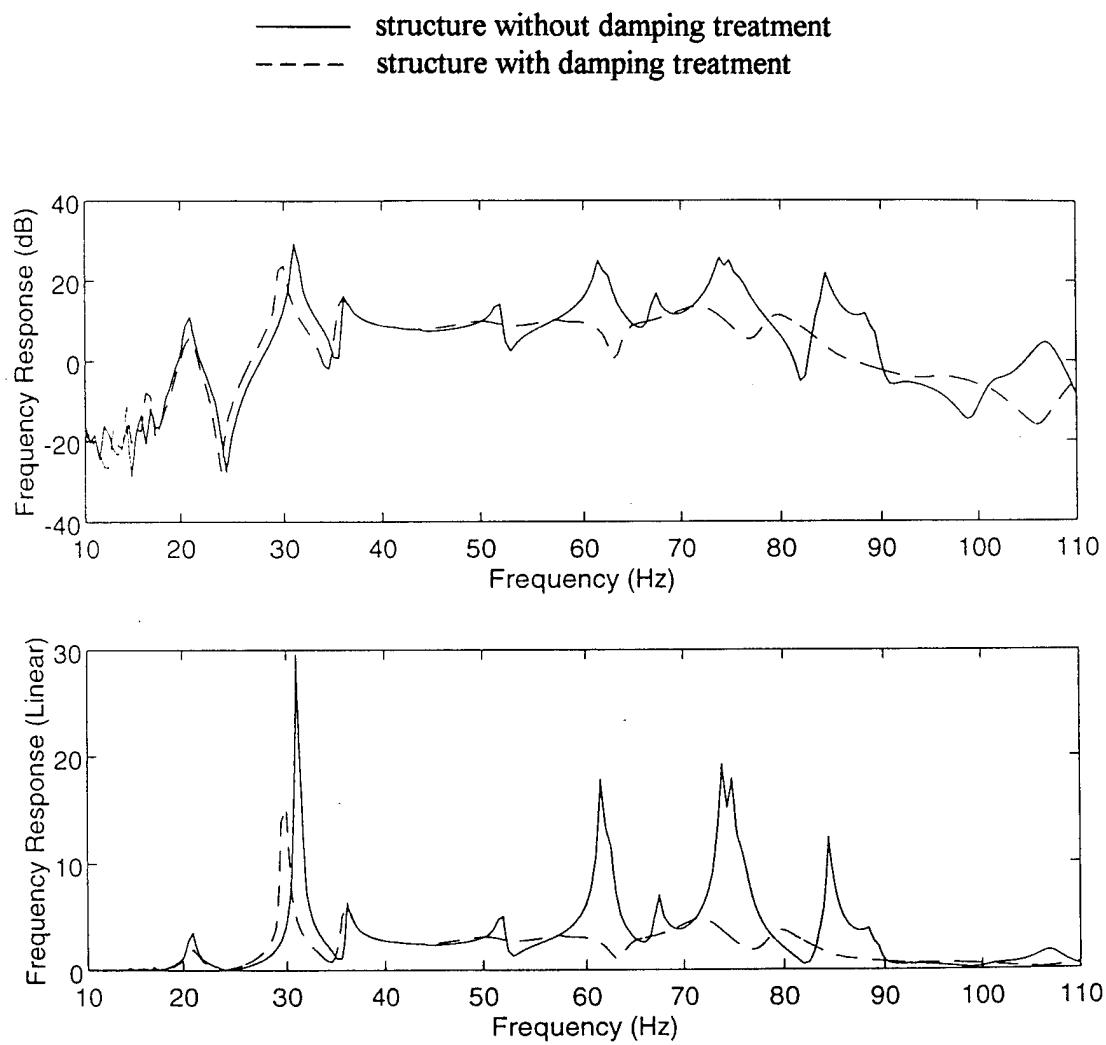
Figure 5.15. Frequency Response: Point K [Front face; (14, 6, 42)].
(*top*: dB scale; *bottom*: Linear scale)

51
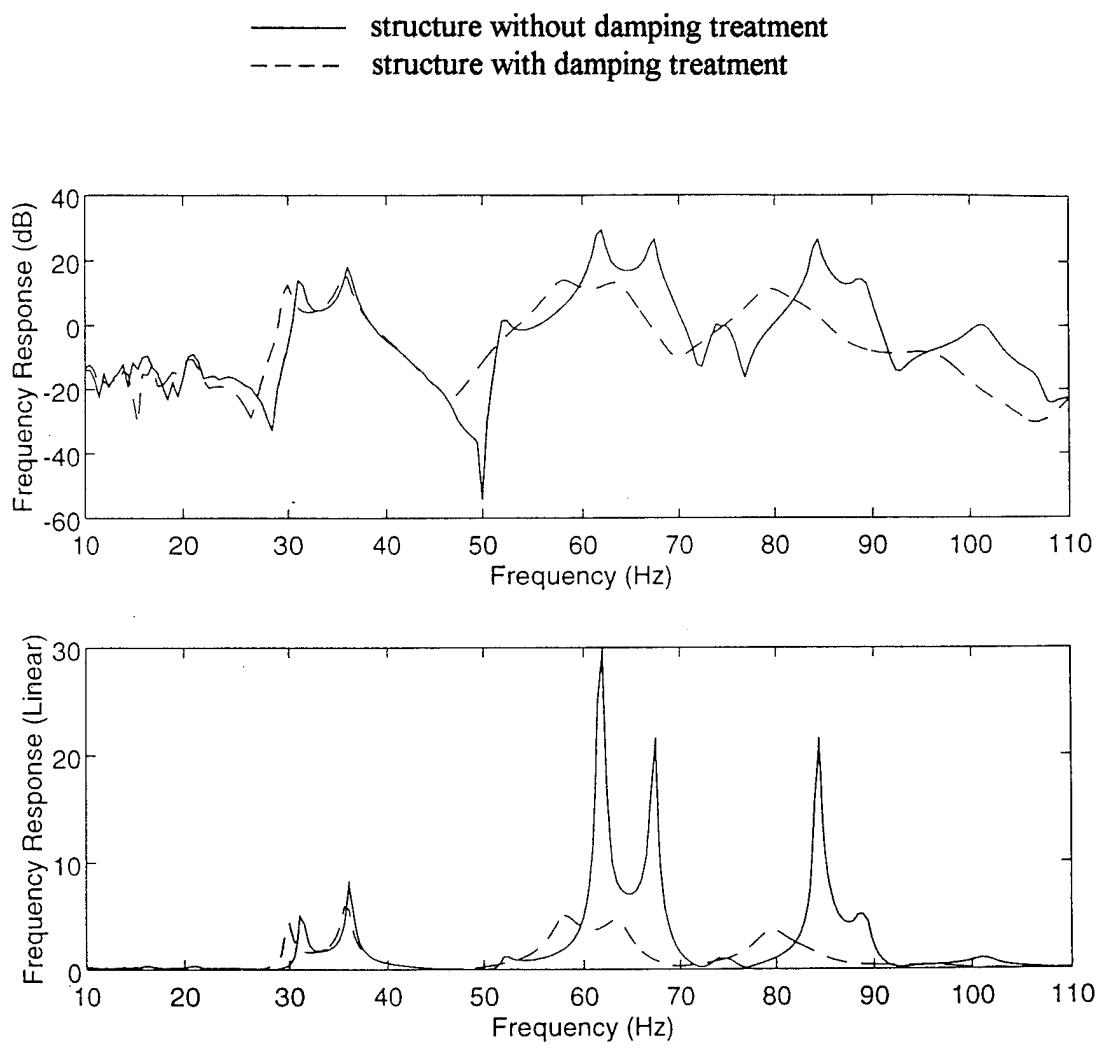
Figure 5.16. Frequency Response: Point M [Back face; (10, 6, 0)].
(*top*: dB scale; *bottom*: Linear scale)

structure without damping treatment
structure with damping treatment
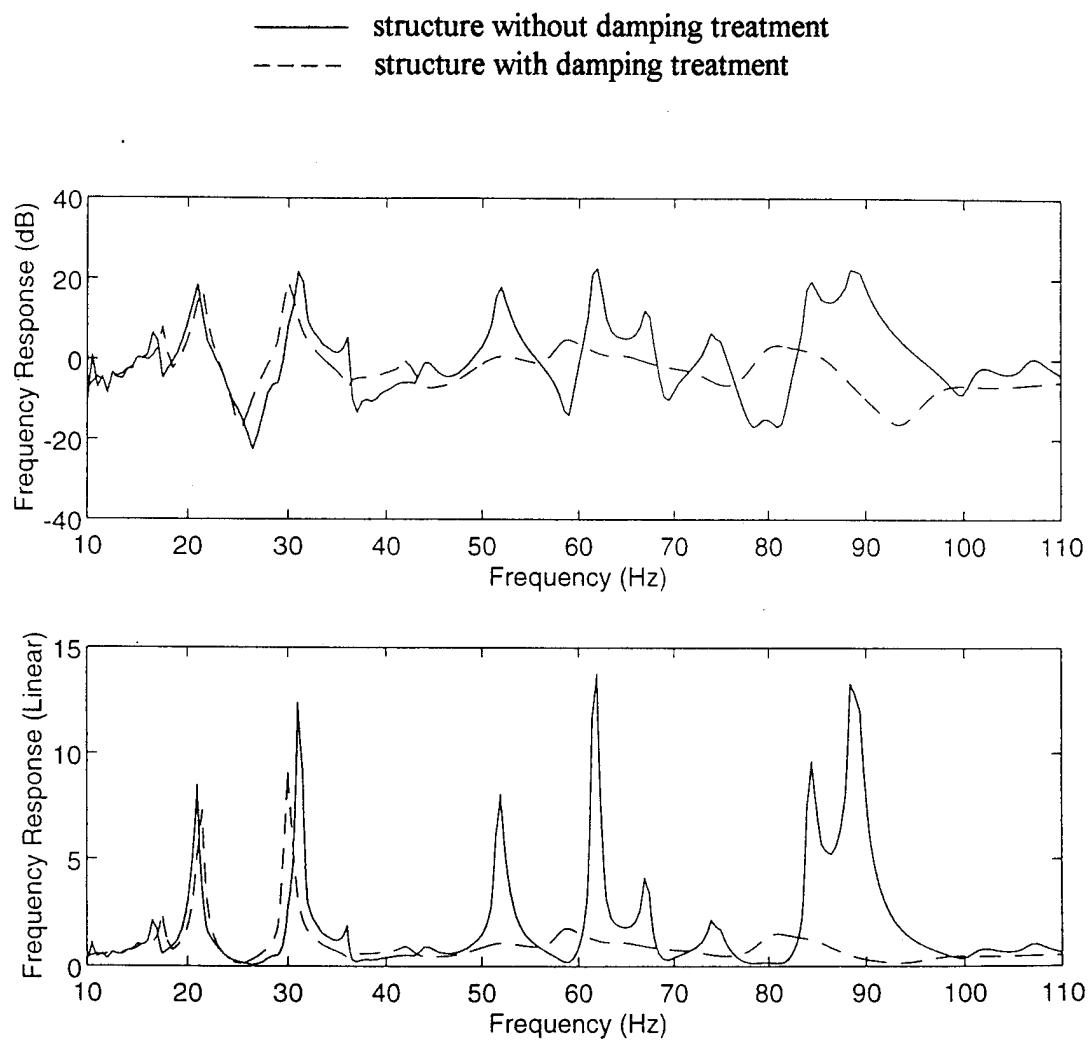
Figure 5.17. Frequency Response: Point N [Bottom; (20, 0, 10)].
(*top*: dB scale; *bottom*: Linear scale)

53

The primary reason for the increased damping at the higher frequencies was due to the fact that a nodal point was exploited at the midspan of both the left and right side of the structure. Also the lower frequency modes of the structure were a system "breathing" type of mode which would require full system coverage of the damping material to effectively dampen.

D.   INTEGRATED SYSTEM ISOLATION AND DAMPING RESULTS

The final step of the experiment was to isolate the vibration generator from the structure by use of sound isolation mounts. This was accomplished by connecting four mounts between the vibration generator support plate and the structure, as shown in Figure 5.18.
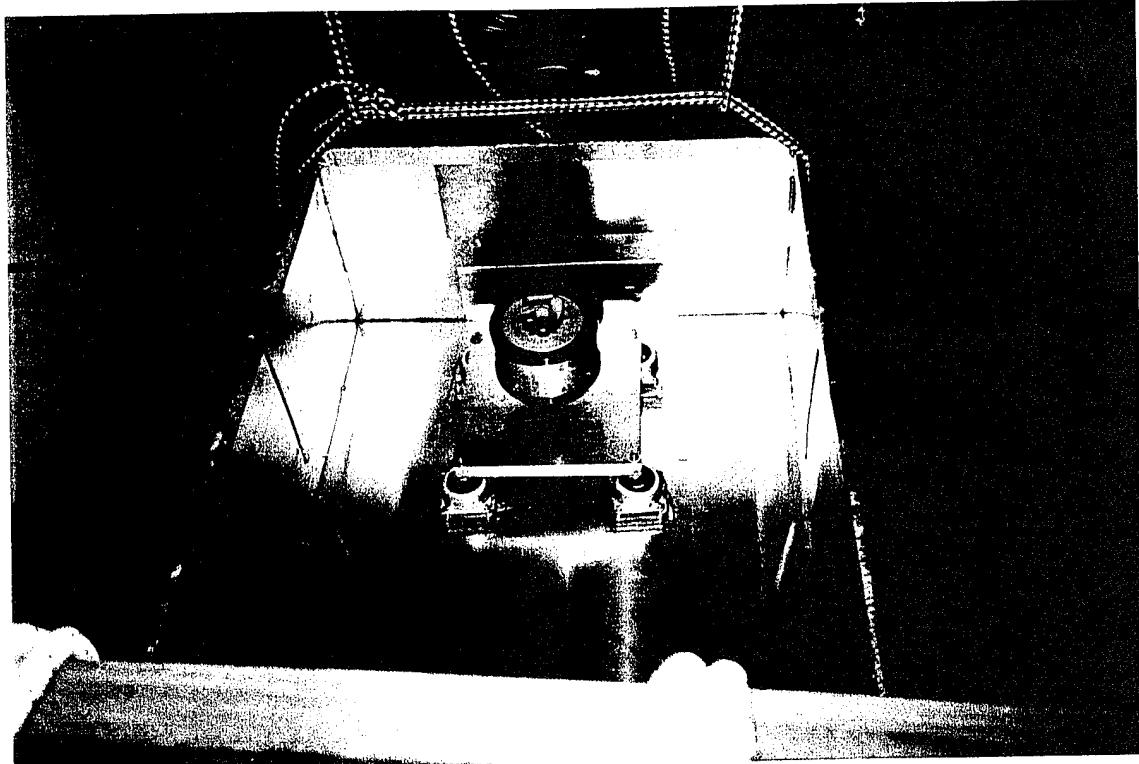
Figure 5.18. Sound Isolation Mounting Configuration.

The mounts used were provided by BARRY CONTROLS of Brighton, MA [Ref. 15]. Table 5.3 provides nominal mount characteristics.

Table 5.3. Isolation Mount Characteristics. [Ref. 15]

Manufacturer	BARRY CONTROLS
Model	L64-BA-6
Static Load Range (lbs)	3 - 6 (per mount)
Natural Frequency (Hz)	7 - 10
Transmissibility at Resonance	2.5
Resilient Element	Friction Damped Spring
Material	Aluminum
Weight (lbs)	0.226 (per mount)

The expected transmissibility, T, as a function of the forcing frequency is illustrated in Figure 5.19. Based on the static load on the mounts, the expected natural frequency of the mount was 9.5 Hz. This mount natural frequency was located close to an analysis structure frequency of 12.05 Hz which could have caused a transmissibility problem, since 12.05 Hz is located in the amplification region for the sound mount. However, the closest experimental structure frequency was 21 Hz, which was located in the isolation region for the mount.
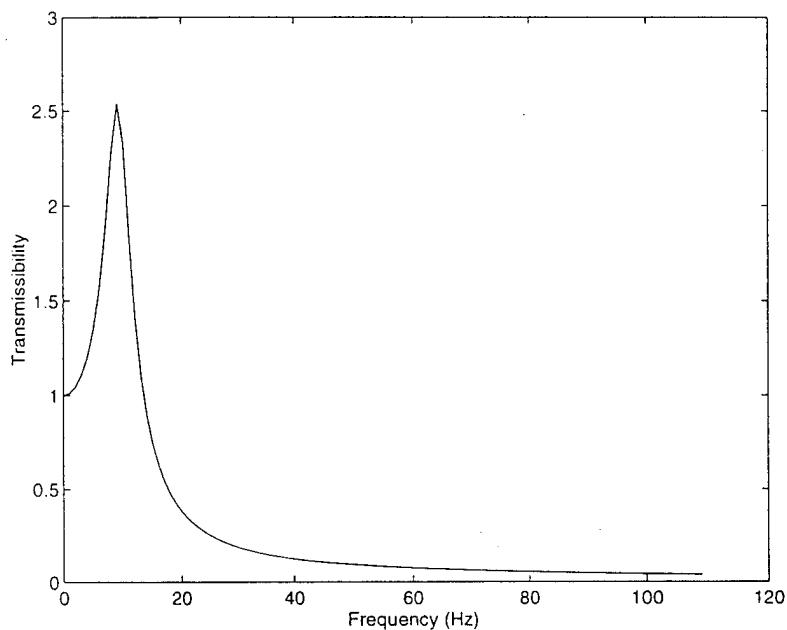
Figure 5.19. Transmissibility as a Function of Forcing Frequency.

After installation frequency response data was obtained at testing points A - O. Examples of frequency response curves are provided in Figures 5.20 through 5.24. This response data is a result of the combined efforts of system constrained viscoelastic layered damping treatment, as well as, source isolation.

structure without damping treatment
structure with damping treatment
structure with damping treatment and source isolation
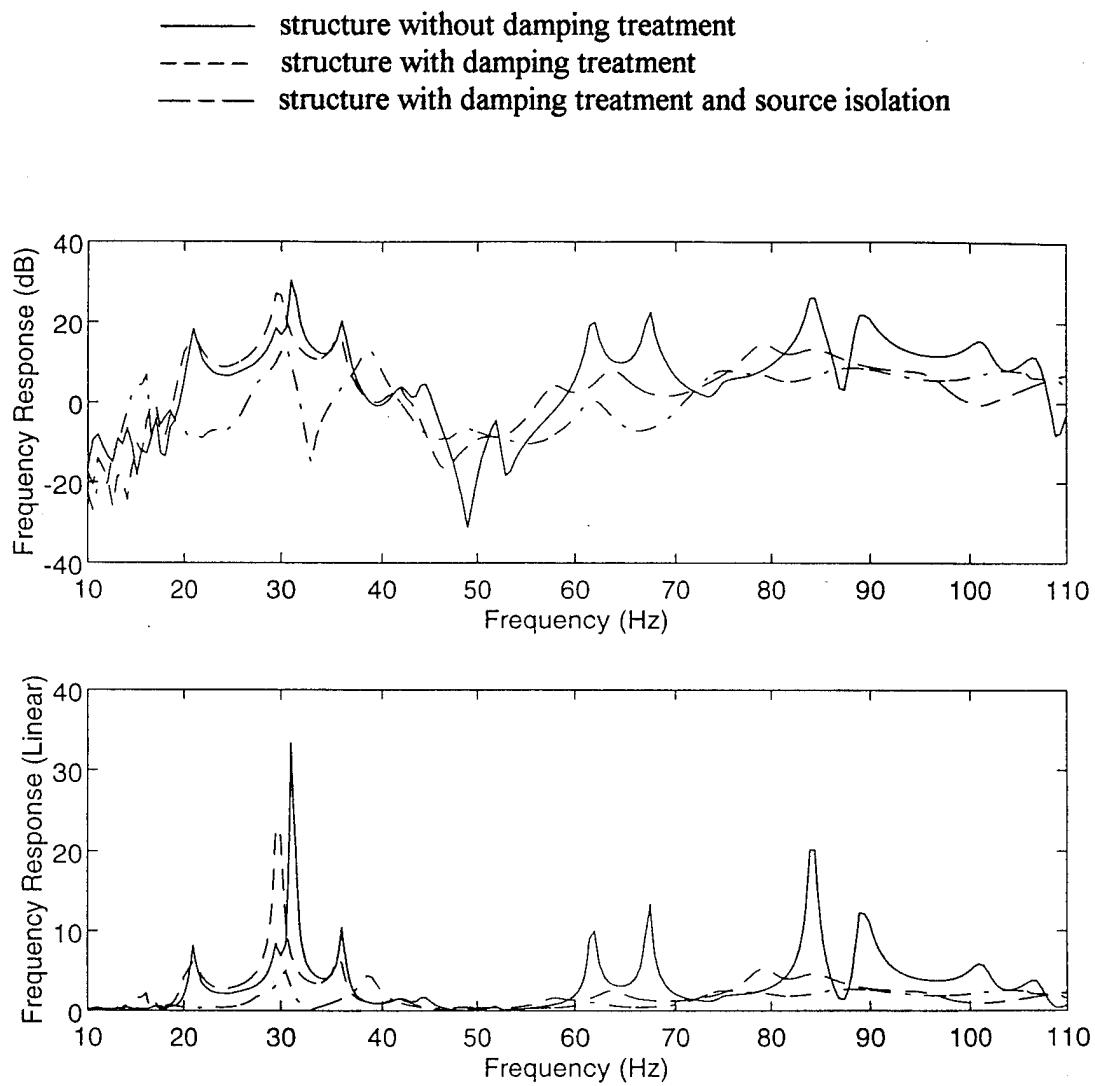
Figure 5.20. Frequency Response: Point E [Left side; (0, 6, 24)].
(*top*: dB scale; *bottom*: Linear scale)

structure without damping treatment
structure with damping treatment
structure with damping treatment and source isolation
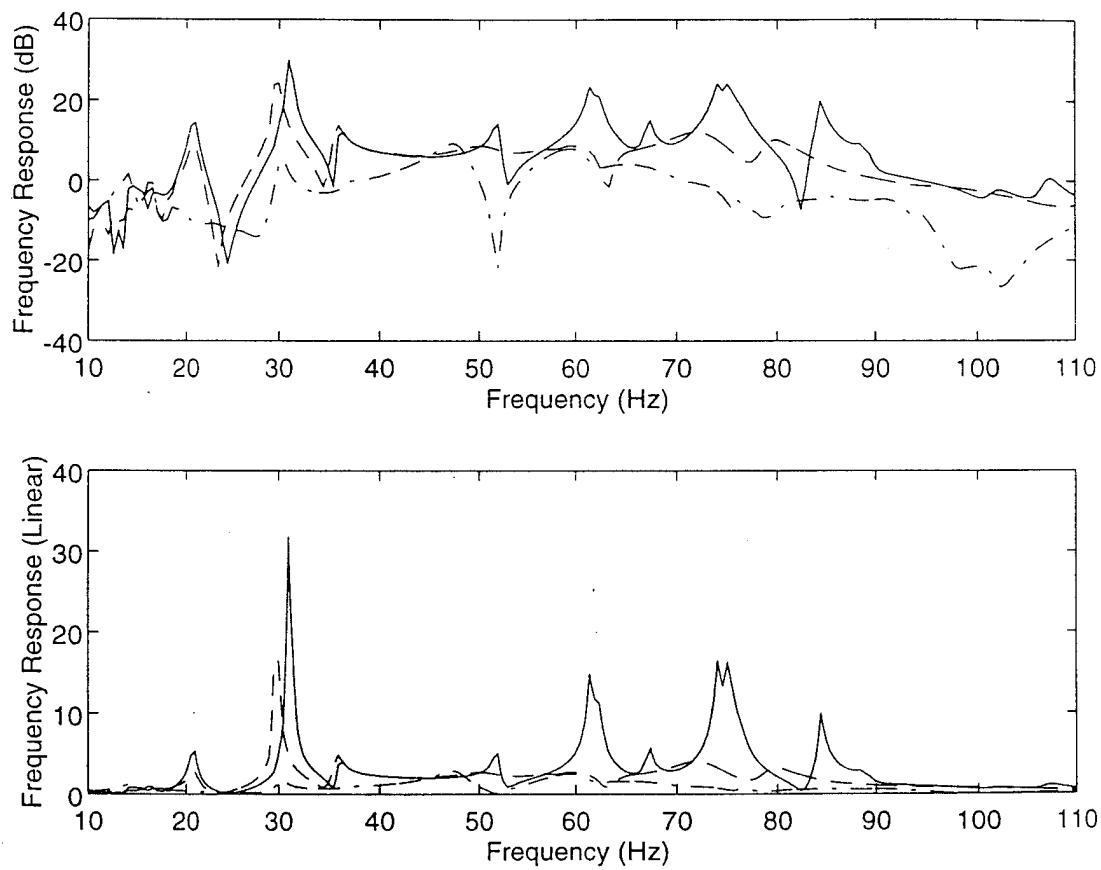
Figure 5.21. Frequency Response: Point J [Front face; (14, 10, 42)].
(*top*: dB scale; *bottom:* Linear scale)
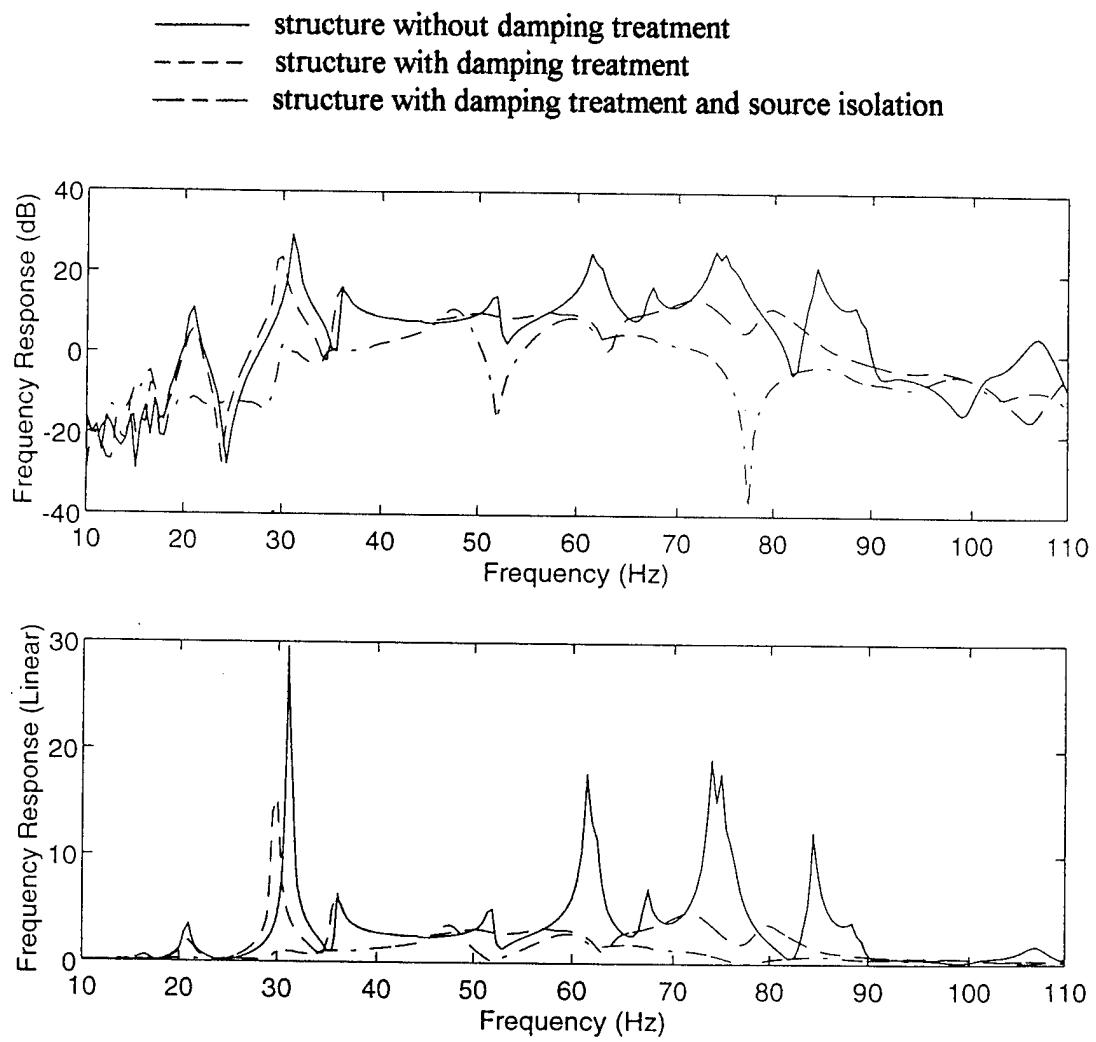
Figure 5.22. Frequency Response: Point K [Front Face; (14,6,42)].
(*top*: dB scale; *bottom*: Linear scale)

structure without damping treatment
structure with damping treatment
structure with damping treatment and source isolation
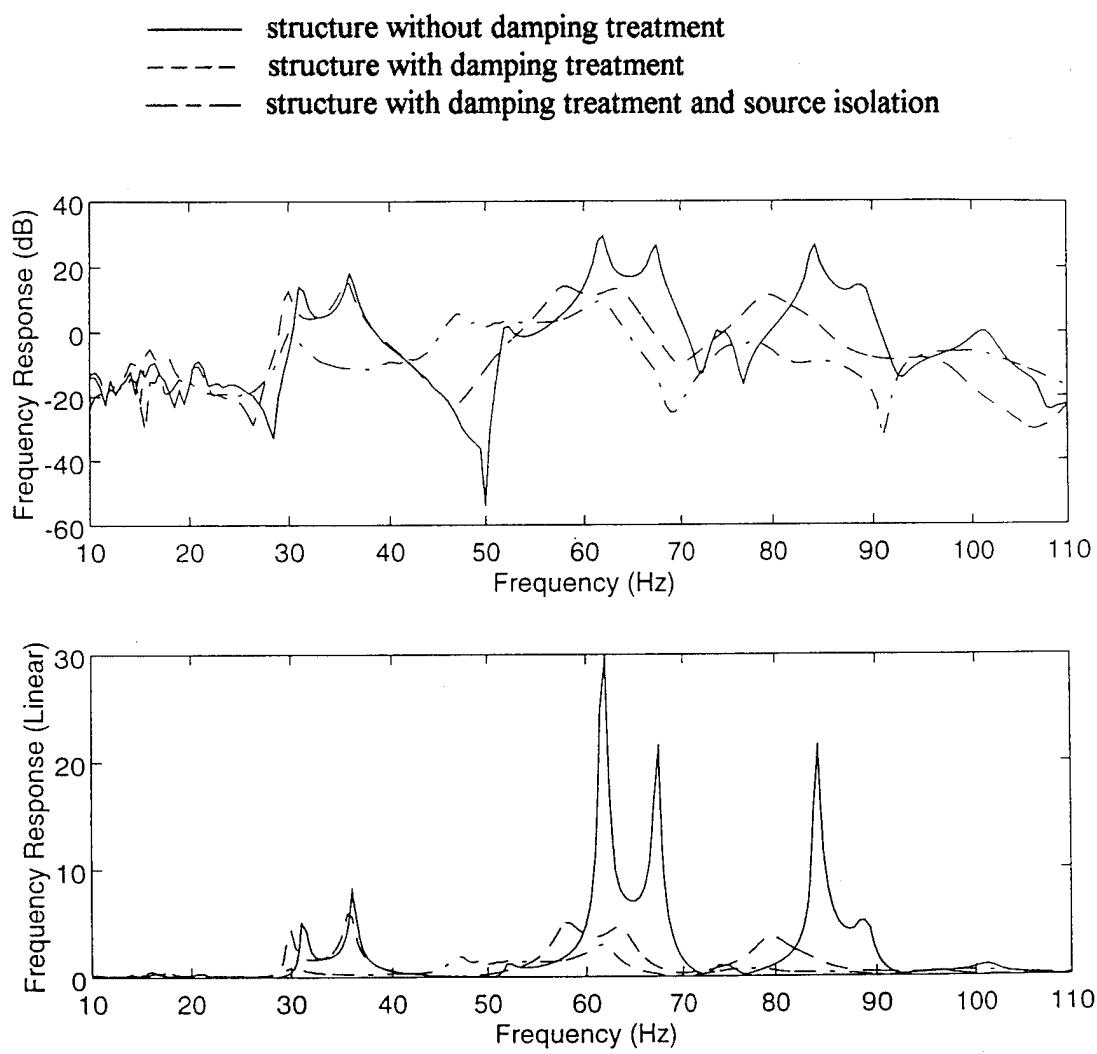
Figure 5.23. Frequency Response: Point M [Back Face; (10, 6, 0)].
(*top*: dB scale; *bottom*: Linear scale)

structure without damping treatment
structure with damping treatment
structure with damping treatment and source isolation
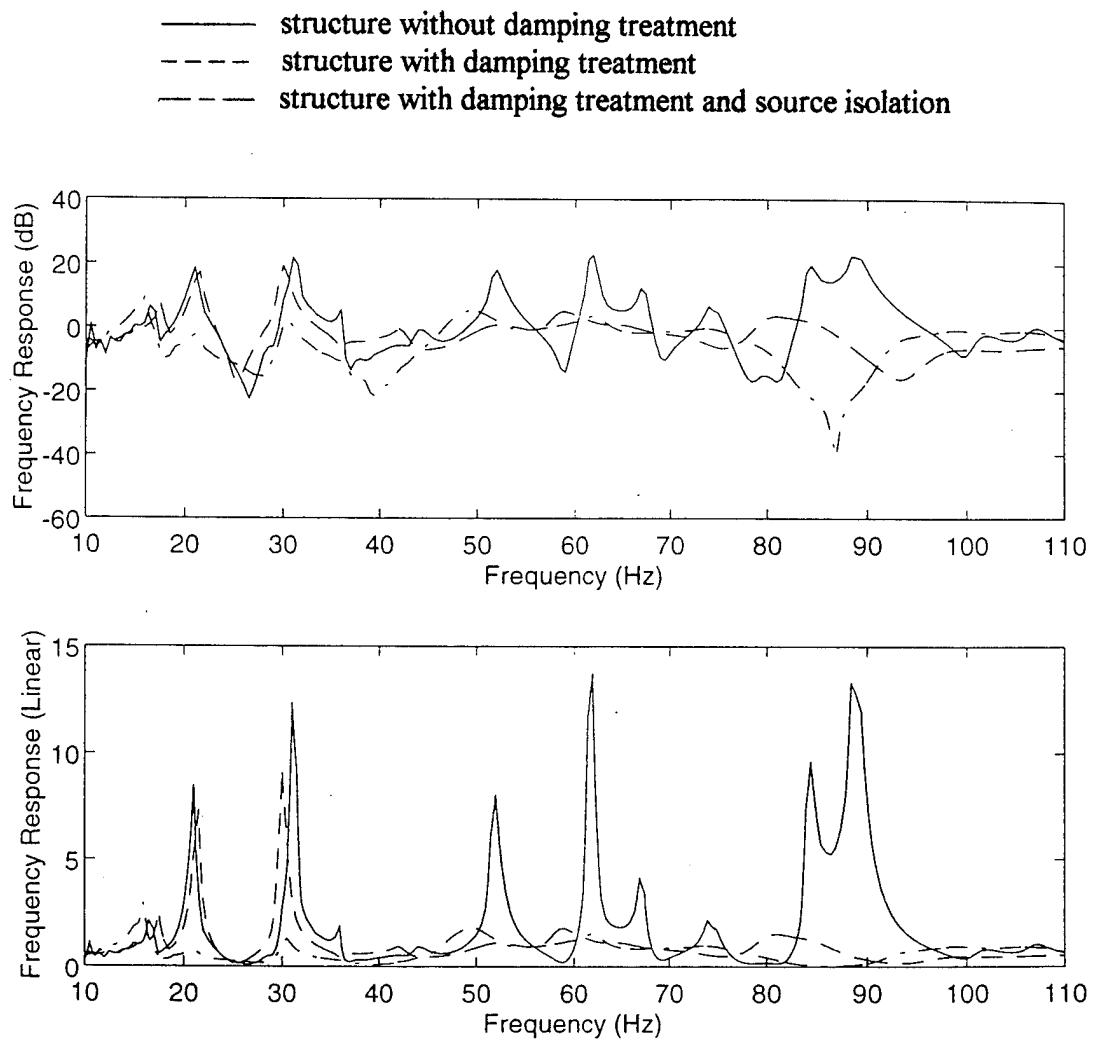
Figure 5.24. Frequency Response: Point N [Bottom; (20, 0, 10)].
(*top*: dB scale; *bottom*: Linear scale)

61

The maximum reduction in the 20 to 50 Hz range was 23.5 decibels (15:1) while the 50 to 80 Hz range experienced a maximum reduction of 26.8 decibels (22:1). The 80 to 100 Hz range also experienced a maximum reduction of 26.8 decibels.

VI. CONCLUSIONS

Constrained viscoelastic layered damping is an effective method of vibration reduction over a broad frequency range. Peak response reductions of 20 decibels were obtained using a very thin layer of viscoelastic material in a partial coverage fashion. Coupling source isolation with system damping yields dramatic reductions in a system vibration signature. A reduction of 26.8 decibels was easily obtained over a 50 Hz span. The viscoelastic damping material and vibration isolator were more effective in suppressing the higher frequency modes (noise related) than the lower frequency modes (displacement related).

An analysis approach in conjunction with limited modal testing allows one to determine locations of high strain energy, as well as, nodal points. These locations are essential in determining placement of damping strips when utilizing a partial coverage technique.

VII. RECOMMENDATIONS

The scope of this work was limited to a single constrained viscoelastic layer damping treatment for a three dimensional structure. There a several areas which deserve more research and clarification, including:

(1) Varying the thickness of the viscoelastic layer to determine the increase in vibration damping capability.

(2) Varying the thickness of the constraining layer to determine the increase in vibration damping capability.

(3) Consider a full surface coverage damping scheme to investigate the net increase in damping capability in addition to comparing experimentally loss values with the values obtained by the RKU equations.

(4) Investigate the use of a double damping layer configuration.

(5) Investigate the effect of damping only the nodal points of the three dimensional structure.

(6) Investigate the use of a tuned damper in conjunction with the constrained viscoelatic layered damping treatment.

(7) Extend the three dimensional analysis to a more complex structure such as the body of an automobile.

APPENDIX A. MATLAB PROGRAM USED TO CALCULATE MODAL LOSS FACTORS FOR THE SINGLE CONSTRAINED VISCOELASTIC LAYERED DAMPING TREATMENT.

This program uses the Ross-Kerwin-Ungar Equations contained in Chapter III to estimate the system modal loss factor for various constrained viscoelastic layered damping configurations. The modal frequency, system temperature, viscoelastic layer thickness, and constraining layer thickness are entered in by the user. Material properties of ISD-112 are computed using University of Dayton data and curve-fitting equations to the reduced frequency nomogram. The units used in this program are pounds, inches, and seconds.

```
%
% Program : Constrained Viscoelastic Damping Design
%
% The purpose of this program is to calculate system loss
% factors for various modes of a constrained layer viscoelastic
% damping system using the ROSS-KERWIN-UNGAR equations. The base
% plate thickness will remain constant at .1 inches. Varying
% temperatures, modal frequencies, viscoelastic thicknesses,
% and constraining layer thicknesses will be entered by the user.
%
% This program applies to an unrestrained structure.
%
% The viscoelastic material is 3M ISD-112.
%
% The following coefficients are defined:
% E1 = Youngs modulus of aluminum base plate (psi)
% E2 = Youngs modulus of viscoelastic material (psi)
% E3 = Youngs modulus of constraining layer (psi)
% v1 = Poissons ratio of base plate
% v2 = Poissons ratio of viscoelastic material
% v3 = Poissons ratio of constraining layer
% rho1 = density of base plate (lbm/in^3)
% rho2 = density of viscoelastic material (lbm/in^3)
% rho3 = density of constraining layer (lbm/in^3)
% f = experimental natural frequency of undamped system (Hz)
% fr1 = reduced system frequency (Hz)
% f1 = calculated frequency of damped system (Hz)
% k1 = system wave number (1/in^4)
% h1 = base plate thickness (in)
% h2 = viscoelastic layer thickness (in)
% h3 = constraining layer thickness (in)
% eta2 = viscoelastic layer loss factor
% nsys = system loss factor
% gc = gravitational constant (lbm-in/s^2-lbf)
% T = system temperature (F)
%
E1=1.02E7;
E3=1.02E7;
v1=.34;
v2=.49;
v3=.34;
rho1=.1;
```

```
rho2=.035;
rho3=.1;
h1=.1;
gc=386.4;
%
% Reduced frequency nomogram variables
T0=104;
from=2e4;
mrom=688.94;
n=.275;
ml=8.7;
etafrol=1.08;
sl=.45;
sh=-.55;
frol=5000;
C=2.5;
f=input('enter sys undamped natural frequency (Hz)   ')
T=input('enter sys temperature (F)   ')
h2=input('enter viscoelastic layer thickness (in)   ')
h3=input('enter constraining layer thickness (in)   ')
%
% determine modal wave number
%
w=2*pi*f;
k1=w*((12*(1-v1^2)*h1*rho1)/(E1*h1^3*gc))^.5;
%
% initialize tolerance
%
tol=.5;
% iteration loop for damped frequency
while tol>=.001
  fr=log10(f)-(12*(T-T0)/(525+T-T0));
  fr1=10^fr;
  A=(fr-log10(frol))/C;
  m=log10(ml)+(2*log10(mrom/ml))/(1+(from/fr1)^n);
  G2=10^m;
  eta=log10(etafrol)+.5*C*(A*(-.1)+(1-(1+A^2)^.5));
  eta2=10^eta;
  E2=G2*2*(1+v2);
  h31=((h1+h3)/2)+h2;
  h21=(h1+h2)/2;
  g=G2/(E3*h3*h2*k1);
```

```
c=E1*h1*(1+g)+g*E3*h3;
d=g*E1*h1*eta2+g*E3*h3*eta2;
ar=g*E1*h1*E3*h3*h31^2*(c+d*eta2);
br=E1*h1*E2*h2*h31*(c+d*eta2);
x=(c*(1-eta2^2)+d*(2*eta2));
cr=2*g*E2*h2*E3*h3*x;
ai=g*E1*h1*E3*h3*h31^2*c*eta2;
bi=E1*h1*E2*h2*h31*(c*eta2-d);
y=(c*2*eta2-d+d*eta2^2);
ci=2*g*E2*h2*E3*h3*h21*h3*y;
EH=E1*h1^3+E3*h3^3;
EH3=EH+(12/(c^2+d^2))*(ar-br-cr);
dens=rho1*h1+rho2*h2+rho3*h3;
f1=(1/(2*pi))*k1*(EH3*gc/(12*(1-v1^2)*dens))^.5;
tol=abs((f-f1)/f);
 f=f1;
end
%
% calculate system loss factor
%
ns=(ai-bi-ci);
nsys=(1/EH3)*(12/(c^2+d^2))*ns;
disp('damped system frequency')
f1
pause
disp('system loss factor')
nsys
pause
```

APPENDIX B. MATLAB PROGRAM USED TO PLOT DSA FREQUENCY RESPONSE DATA.

The frequency response data sent from the DSA to the data acquisition computer is a set of real and imaginary points. This program calculates the magnitude of the data and plots it in dB or linear form.

```
% PROGRAM : DATA CONVERSION
%
% THE PURPOSE OF THIS PROGRAM IS TO CONVERT DSA FREQUENCY
% RESPONSE RAW DATA ( A SET OF REAL AND IMAGINARY POINTS)
% TO DATA THAT CAN BE PLOTTED IN MATLAB ON A LINEAR OR
% dB SCALE.
%
% a = raw data points
%

k=1;
j=2;
for i=1:1:801
 R(i)=a(k);
 k=k+2;
end
for i=1:1:801
 I(i)=a(j);
 j=j+2;
end
for i=1:1:801
 m(i)=(R(i)^2+I(i)^2)^.5;
end
step=100/801;
f=[10:step:110-step];
for i=1:1:801
 d(i)=20*log10(m(i));
end
subplot(211),plot(f,d)
subplot(211),xlabel('Frequency (Hz)')
subplot(211),ylabel('Frequency Response (dB)')
subplot(212),plot(f,m)
subplot(212),xlabel('Frequency (Hz)')
subplot(212),ylabel('Frequency Response (Linear)')
```

LIST OF REFERENCES

1. Rao, S. S., <u>Mechanical Vibrations</u>, 3rd Edition, Addison - Wesly Publishing Company, 1995.

2. Azvine, B., and Wynne, R. J., "Active Damping for the Control of Flexible Structures", Vibration Control Conference Publication #389, March 1994.

3. Barron, R., "Control Strategies in the Active Isolation of Engineering Systems", Vibration Control Conference Publication. #389, March 1994.

4. Shin, Y. S., and Maurer, G. J.,"Vibration Response of Constrained Viscoelastically Damped Plates: Analysis and Experiments", Elsevier Science Publishers, 1991.

5. Bateman, M. J., <u>Constrained Viscoelastic Layer Damping of Thick Aluminum Plates: Design, Analysis, and Testing</u>, M. S. Thesis, U.S. Naval Postgraduate School, Monterey, California, March 1990.

6. Nashin, A. D., Jones, D.I.G., and Henderson, J. P., <u>Vibration Damping</u>, Wiley - Interscience Publications, John Wiley and Sons, 1985.

7. Jones, D.I.G., and Henderson, J. P., "Fundamentals of Damping Materials", Vibration Damping Short Course Notes, Section 2.3, University of Dayton, Dayton, Ohio, June 1987.

8. Rogers, L., "Single Constrained Layer Damping Treatment Analysis", Vibration Damping Short Course Notes, Section 6.3, University of Dayton, Dayton, Ohio, June 1987.

9. Beranek, L. L., <u>Noise and Vibration Control</u>, Institute of Noise Control Engineering, 1988.

10. Lawry, M. H., *I-DEAS^{TM} Student Guide*, Structural Dynamics Research Corporation, 1994.

11. Drake, M. L., "Modified Ross,Kerwin,and Ungar Techniques", Vibration Damping Short Course Notes, Section 7, University of Dayton, Dayton, Ohio, June 1987.

12. Hewlett-Packard Co., 3562A DYNAMIC SIGNAL ANALYZER Operating Manual, Hewlett-Packard Co., 1985.

13.   Wilcoxon Research, PIEZOELECTRIC/ELECTROMAGNETIC Vibration Generator System (MODEL F7/F4) Instruction Manual, Wilcoxon Research, 1985.

14.   Wilcoxon Research, SHAKER POWERING SYSTEMS (MODEL PA7 and MODEL N7/N9) Operating Guide, Wilcoxon Research, 1985.

15.   Barry Controls, "Vibration, Shock, and Noise", Applied Power Inc., 1993.

INITIAL DISTRIBUTION LIST

No. of Copies

1. Defense Technical Information Center 2
8725 John J. Kingman Rd., STE 0944
Ft. Belvoir, VA 22060-6218

2. Dudley Knox Library 2
Naval Postgraduate School
411 Dyer Rd.
Monterey, CA 93943-5101

3. Department Chairman, Code ME/Mz 1
Department of Mechanical Engineering
Naval Postgraduate School
Monterey, CA 93943

4. Naval Engineering Curricular Office, Code 34 1
Naval Postgraduate School
Monterey, CA 93943

5. Professor Y. S. Shin, Code ME/Sg 2
Department of Mechanical Engineering
Naval Postgraduate School
Monterey, CA 93943

6. LCDR James A. Speer 2
2656 Twisted Oak Cove South
Cordova, Tennessee 38018